PCCP

ROYAL SOCIETY OF CHEMISTRY

PAPER

View Article Online
View Journal | View Issue

Check for updates

Cite this: *Phys. Chem. Chem. Phys.*, 2023, **25**, 22063

Improved reweighting protocols for variationally enhanced sampling simulations with multiple walkers†

Baltzar Stevensson * and Mattias Edén *

In molecular dynamics simulations utilizing enhanced-sampling techniques, reweighting is a central component for recovering the targeted ensemble averages of the "unbiased" system by calculating and applying a bias-correction function $c(t)$. We present enhanced reweighting protocols for variationally enhanced sampling (VES) simulations by exploiting a recent reweighting method, originally introduced in the metadynamics framework [Giberti *et al. J. Chem. Theory Comput.*, 2020, **16**, 100–107], which was modified and extended to multiple-walker simulations: these may be implemented either as "independent" walkers (associated with one unique correction function per walker) or "cooperative" ones that all share one correction function, which is the hitherto only explored option. When each case is combined with the two possibilities of determining $c(t)$ by time integration up to either t or over the entire simulation period $\mathcal{T}$, altogether four reweighting options result. Their relative merits were assessed by well-tempered VES simulations of two model problems: locating the free-energy difference between two metastable molecular conformations of the *N*-acetyl-L-alanine methylamide dipeptide, and the recovery of an *a priori* known distribution when one water molecule in the liquid phase is perturbed by a periodic free-energy function. The most rapid convergence occurred for large cooperative walkers, regardless of the upper integration limit, but integrating up to t proved advantageous for small walker ensembles. That novel reweighting method compared favorably to the standard VES reweighting, as well as to current state-of-the-art reweighting options introduced for metadynamics simulations that estimate $c(t)$ by integration over the collective variables. For further gains in computational speed and accuracy, we also introduce analytical solutions for $c(t)$, as well as offering further insight into its features by approximative analytical expressions in the "high-temperature" regime.

Received 29th August 2022,
Accepted 2nd July 2023

DOI: 10.1039/d2cp04009c

rsc.li/pccp

Open Access Article. Published on 03 July 2023. Downloaded on 1/21/2026 10:11:48 PM.
This article is licensed under a Creative Commons Attribution 3.0 Unported Licence.

1. Introduction

Enhanced sampling (ES) techniques for molecular dynamics (MD) simulations, such as umbrella sampling,[1,2] replica exchange,[3,4] and steered MD[5,6] along with the more recent options of metadynamics,[7–16] variationally enhanced sampling (VES),[17–23] and machine learning,[24–26] offer powerful means to accelerate the convergence of MD simulations *via* an enhanced free-energy surface-sampling by avoiding that states are revisited. Hence, they may address challenging systems featuring multiple local energy minima separated by high barriers that would require a prohibitive time-scale by classical MD simulations. This is accomplished by adding a time-dependent *bias potential*, $V(s, t)$, which depends on a set of *collective variables* (CVs) of the system, denoted by s.[7–13]

Numerous refinements of ES protocols have been presented, encompassing the precise choices of CVs[14,16,23,24,26–28] and bias-potential parametrization,[10,15,22,29,30] along with miscellaneous very recent options,[27,31,32] as well as improved *reweighting* procedures[12,33–38] to recover the targeted *unbiased* free energy, $F(s)$, from the sum $F(s) + V(s, t)$ that governs the *biased* MD trajectory.

In particular metadynamics has been widely applied for modeling (bio)chemical processes, such as the nucleation and growth of carbon nano-tubes,[39–41] proton transfers,[42–44] conformations of biomolecules in solution,[28,45–47] as well as their binding at inorganic surfaces.[48–50] Also the herein utilized VES procedure[17–23] has been employed for modeling of molecular conformations in solutions,[18,51] crystal nucleation,[21,30] whereas the ability of VES to handle large sets of CVs have enabled simulations of protein folding.[22,52]

Two powerful options for accelerating the convergence of the ensemble-averaged free energy and other observables from ES/MD simulations involve either (I) calculation of the time-dependent bias-correction function, $c(t)$, by analyzing non-equilibrated

Department of Materials and Environmental Chemistry, Stockholm University, SE-106 91 Stockholm, Sweden. E-mail: baltzar.stevensson@mmk.su.se, mattias.eden@mmk.su.se

† Electronic supplementary information (ESI) available. See DOI: https://doi.org/10.1039/d2cp04009c

Open Access Article. Published on 03 July 2023. Downloaded on 1/21/2026 10:11:48 PM.
This article is licensed under a Creative Commons Attribution 3.0 Unported Licence.

systems using *time* integration, as in the very recent "iterative trajectory reweighting" (ITRE) algorithm introduced for metadynamics simulations by Giberti *et al.*,[38] or (II) an enhanced simultaneous sampling of the CV space by performing multiple (N_W) computations in parallel, each referred to as a "*walker*" and subjected to the same bias potential.[10,14,16,19,27,46,53] Using several such walkers may greatly accelerate the convergence of ES/MD simulations.[10,14,16,19,27,53] For multiple-walker ES simulations, we introduce the concepts of "*independent*" and "*cooperative*" walkers, which are associated with N_W distinct bias-correction functions $\{c_w(t)\}$, and one shared $c(t)$ function [denoted by $c_\Sigma(t)$], respectively; see Section 3. Section 2 outlines the salient features of VES and reweighting, moreover reviewing the hitherto (probably) most efficient and accurate options for determining $c(t)$.[36–38]

By coupling options (I) and (II)—and thereby generalizing a modified ITRE protocol to multiple-walker simulations and integrating it with the VES framework[17–19,23]—we demonstrate that an overall accelerated convergence results relative to the reweighting procedure of the original VES protocol.[17–20] The latter is moreover shown to be equivalent to the balanced exponential (BE) reweighting of Schäfer and Settanni[37] when implemented within the VES scope. Our proposed reweighting method was selected from assessments of four new protocols for estimating $c(t)$ by combining the options of (A) independent or cooperative walker ensembles with (B) estimations of $c(t)$ by time-integration up to either t or across the entire MD simulation time period ($\mathcal{T}$). The convergence properties of the altogether four distinct reweighting procedures were evaluated for two model problems (Section 5): (i) locating the free-energy difference between two metastable molecular conformations of the *N*-acetyl-L-alanine methylamide dipeptide, which is a widely exploited system for benchmarking ES developments.[12,14,17,26,27,36,37,54] (ii) The convergence to a known distribution when one water molecule in the liquid phase is subjected to a known (artificial) free-energy perturbation.

We discuss the relative merits of the novel reweighting options for "small" and "large" ensembles of both cooperative and independent walkers for well-tempered VES implementations with both "good" and "poor" collective-variable selections, the choice of which strongly affects the convergence of the computed ensemble-averaged observables. Nonetheless because an optimal choice of collective variable often remains *a priori* unknown, simulation protocols that simultaneously offer quick convergence and high accuracy even for unfavorable collective variables are desirable. The overall most rapid convergence resulted for simulations with cooperative walkers combined with $c(t)$ calculated by time integration up to t (rather than to $\mathcal{T}$). That herein advocated "M^t_Σ" procedure compared favorably *both* to the standard reweighting procedure in VES[17–19] and the state-of-the-art reweighting metadynamics protocol by Tiwary and Parrinello[36] (when implemented within VES). For further computational speed and accuracy enhancements, we also provide analytical solutions for the $c(t)$ function of the M^t_Σ protocol (Section 3.2). These time savings and accuracy-boosts are expected to be of great utility for further ES/MD-simulation studies.

2. Theoretical background

2.1 Ensemble-averaged observables from biased trajectories

The ensemble average $\langle O(R)\rangle$ of an observable $O(R)$ that depends on spatial coordinates R is defined[7–10,14,16,19,55]

$$\langle O(R)\rangle = \frac{\int \mathrm{d}R O(R)\exp\{-\beta U(R)\}}{\int \mathrm{d}R\,\exp\{-\beta U(R)\}}. \tag{1}$$

It may be calculated according to

$$\langle O(R)\rangle = \frac{Z_V}{Z}\frac{\int \mathrm{d}R O(R)\exp\{-\beta[U(R)+V(s(R),t)]\}\,\exp\{\beta V(s(R),t)\}}{Z_V}, \tag{2}$$

where $U(R)$ is the internal energy of the system, and $\beta = (k_B T)^{-1}$, where k_B and T are Boltzmann's constant and the absolute temperature, respectively. The partition functions of the *biased* (Z_V) and *unbiased* (Z) ensembles are given by

$$Z_V = \int \mathrm{d}R \exp\{-\beta[U(R)+V(s(R),t)]\}, \tag{3}$$

and

$$Z = \int \mathrm{d}R\,\exp\{-\beta U(R)\}, \tag{4}$$

respectively.

The *unbiased probability distribution*, $P(s)$, is defined by

$$P(s) = \frac{\int \mathrm{d}R \delta(s-s'(R))\exp\{-\beta U(R)\}}{\int \mathrm{d}R \exp\{-\beta U(R)\}}, \tag{5}$$

where $\delta(x)$ is the Dirac delta function. After integration over R, the probability distribution may be expressed as

$$P(s) = Z^{-1}\exp\{-\beta F(s)\}, \tag{6}$$

where "s" implies either that the collective variable(s) is/are independent on spatial coordinates or depend(s) only on a specifically selected subset thereof. The introduction of the two $\exp\{\pm\beta V(s(R),t)\}$ factors in eqn (2) along with the multiplication of both its nominator and denominator by Z_V implies that the *biased* simulation sample configurations from the $V(s,t)$-biased probability distribution,[7–10,14,16,19]

$$P_V(s,t) = Z_V{}^{-1}\exp\{-\beta[F(s)+V(s,t)]\}. \tag{7}$$

By equating the ratio Z_V/Z of eqn (2) with the exponentiated bias-correction function, *i.e.*, $Z_V/Z = \exp\{-\beta c(t)\}$, eqn (2) may be written

$$\langle O(R)\rangle = \frac{\int \mathrm{d}R O(R)\exp\{-\beta[U(R)+V(s(R),t)]\}\exp\{\beta[V(s(R),t)-c(t)]\}}{\int \mathrm{d}R\,\exp\{-\beta[U(R)+V(s(R),t)]\}}. \tag{8}$$

 This journal is © the Owner Societies 2023

Open Access Article. Published on 03 July 2023. Downloaded on 1/21/2026 10:11:48 PM. This article is licensed under a Creative Commons Attribution 3.0 Unported Licence.

By assuming ergodicity—*i.e.*, a time/ensemble-averaging equivalence, $\langle O(R)\rangle$ may be estimated from the *time*-average over the biased MD-generated trajectory, according to[7–10,14,16,19,27,36–38]

$$\langle O(R)\rangle = \frac{\int \mathrm{d}t O(R(t)) \exp\{\beta[V(s(t),t) - c(t)]\}}{\int \mathrm{d}t \exp\{\beta[V(s(t),t) - c(t)]\}}. \quad (9)$$

Eqn (9) is the prevailing route to calculate ensemble averages from ES simulations, where the calculation of $c(t)$ becomes the central task for recovering $F(s)$ and $\langle O(R)\rangle$ from the biased trajectories.[7–10,14,16,19]

Moreover, for a well-tempered ensemble over a sufficiently long time, the bias potential $V(s, t)$ is related to $F(s)$ *via* the bias factor γ by[11–15,19,20]

$$V(s, t) = -(1 - \gamma^{-1})F(s), \quad (10)$$

whereas $P_V(s, t)$ [eqn (7)] is related to $P(s)$, according to

$$P_V(s, t) = \frac{[P(s)]^{1/\gamma}}{\int \mathrm{d}s [P(s)]^{1/\gamma}}. \quad (11)$$

2.2 Variationally enhanced sampling

The variationally enhanced sampling[17–23] protocol aims at minimizing a bias-potential-dependent functional, $\Lambda(V(s, t))$, which for a time-dependent bias potential, $V(s, t)$, and a well-tempered target distribution, $P_V(s, t)$ (eqn (11)) is given by[17,19–21]

$$\Lambda(V(s,t)) = \beta^{-1} \ln\left\{\frac{\int \mathrm{d}s \exp\{-\beta[F(s) + V(s,t)]\}}{\int \mathrm{d}s \exp\{-\beta F(s)\}}\right\} + \frac{\int \mathrm{d}s V(s,t)[P(s)]^{1/\gamma}}{\int \mathrm{d}s [P(s)]^{1/\gamma}}. \quad (12)$$

The global minimum of the convex functional $\Lambda(V(s, t))$ is[18,19]

$$V(s, t) = -F(s) - (\beta\gamma)^{-1} \ln P(s) - \beta^{-1} \ln Z_V. \quad (13)$$

For practical computations, the bias potential is expanded in a suitable set of k basis functions, whose corresponding $\{\alpha_k\}$ expansion coefficients are the variational parameters that are updated iteratively during the minimization of $\Lambda(V(s, t))$.[17,19–22] For the present calculations that involve s-periodic bias potentials, we employed a combined cosine and sine Fourier series,

$$V(s,t) = \alpha_0 + \sum_{k=1}^{N_F} \alpha_{2k-1}(t)\cos\{ks\} + \alpha_{2k}(t)\sin\{ks\}, \quad \text{with } 0 \le s < 2\pi, \quad (14)$$

where $\alpha_0 = 0$ in previous[17–23] as well as our current VES implementations.

With the recent exception of Yang and Parrinello,[23] who combined the time-lagged independent component analysis[56] and VES, all previous reweighting implementations were tantamount to using a *constant* bias-correction function, *i.e.*, effectively $c(t) = 0$, which only holds *strictly* for "late" time-points of the MD simulation; see Sections 2.3.1, 3.1 and 5.3. Herein, we demonstrate that state-of-the-art reweighting procedures from the metadynamics context that employ time-dependent bias-correction functions[36,38] may offer both a more rapid and a reliable convergence of the modeled observables relative to the standard VES reweighting implementation with $c(t) = 0$.

2.3 Efficient strategies for calculating the time-dependent bias correction

Here we review current state-of-the-art approaches—all from the realm of (well-tempered) metadynamics—for estimating the bias-potential-correction function by integrating either over collective variables[36,37] or over time.[38,54]

2.3.1 Integration over collective variables. Tiwary and Parrinello[36] showed that $c(t)$, expressed by an integration over the entire CV space,

$$c(t) = -\beta^{-1} \ln\left\{\frac{\int \mathrm{d}s \exp\{-\beta[F(s) + V(s,t)]\}}{\int \mathrm{d}s \exp\{-\beta F(s)\}}\right\}, \quad (15)$$

may be estimated by using the well-tempered relation for the free energy

$$F(s) = \frac{-V(s,t)}{1 - \gamma^{-1}} + \beta^{-1} \ln\left\{\int \mathrm{d}s \exp\{\beta V(s,t)/(1 - \gamma^{-1})\}\right\}. \quad (16)$$

Becuase eqn (16) is only exact once the entire CV space is sampled, which formally demands that $t \to \infty$, reweighting *via* eqn (15) and (16) remains accurate after a "transient" time period on a (sub)ns scale,[19,36] where the *a priori* unknown lower limit is herein denoted by t_{min}. The calculations may otherwise introduce non-negligible errors and no universal and truly accurate procedure accounting for the unpopulated CV values is hitherto presented. Notably, as illustrated in Section 5.2, the same caveat applies to the standard VES reweighting (Sections 2.2 and 3.1).

The combination of eqn (15) and (16) is the key feature of the procedure by Tiwary any Parrinello[36] for estimating $c(t)$ *via* an integration over the CVs; it is henceforth denoted by M_Σ^{TP}, and is associated with a bias-potential-correction function $c_\Sigma^{TP}(t)$ obtained from eqn (15), where the subscript Σ stresses the use of cooperative walkers for multi-walker simulations. We have successfully utilized the Tiwary–Parrinello reweighting protocol within the VES formalism for studying biomolecular binding at calcium phosphate surfaces.[57,58]

Schäfer and Settanni[37] suggested by their "balanced exponential" protocol that a better estimate of $c(t)$ [eqn (15)] may be obtained, associated with the readily calculated bias-correction function given by the average value of $V(s,t)$ over the CVs:[37]

$$c(t) = \frac{\int \mathrm{d}s V(s,t)}{\int \mathrm{d}s}. \quad (17)$$

Metadynamics simulations utilizing reweighting by the BE procedure compared favorably[37] with that of Tiwary and Parrinello,[36] as well as with an earlier option introduced by Bonomi *et al.*[12] (the latter is not considered further herein). Incidentally, for VES implementations with $V(s,t)$ expressed according to eqn (14), then eqn (17) evaluates to

$$c(t) = \alpha_0 = 0. \quad (18)$$

Open Access Article. Published on 03 July 2023. Downloaded on 1/21/2026 10:11:48 PM.
This article is licensed under a Creative Commons Attribution 3.0 Unported Licence.

Hence, the bias-correction function from the metadynamics-stemming BE reweighting coincides with that of VES. Consequently, we will in the following refer to this reweighting method as $M_{\Sigma}^{\mathrm{VES}}$ but we will cite both ref. 17 and 37 to emphasize that once the BE reweighting is applied within the VES context, it reduces to the "standard" VES reweighting with a time-*independent* bias-correction function.

2.3.2 Integration over time. Giberti *et al.*[38] recently introduced the ITRE reweighting procedure for calculating $c(t)$ and $F(s)$ from metadynamics simulations, which they argued gives significant benefits to s-integration-based reweighting counterparts, such as those of ref. 12, 19 and 36. The ITRE protocol estimates $F(s)$ from the unbiased distribution by integrating eqn (9) up to time-point t (Fig. 1a),

$$P(s,t) = \exp\{-\beta F(s)\} = \frac{\int_0^t \mathrm{d}\tau \delta(s-s'(\tau))\exp\{\beta[V(s'(\tau),\tau)-c(\tau)]\}}{\int_0^t \mathrm{d}\tau\, \exp\{\beta[V(s'(\tau),\tau)-c(\tau)]\}}, \quad (19)$$

whereupon combination of eqn (15) and (19) yields the expression[38]

$$\exp\{-\beta c(t)\} = \frac{\int_0^t \mathrm{d}\tau\, \exp\{\beta[V(s(\tau),\tau)-c(\tau)-V(s(\tau),t)]\}}{\int_0^t \mathrm{d}\tau\, \exp\{\beta[V(s(\tau),\tau)-c(\tau)]\}}. \quad (20)$$

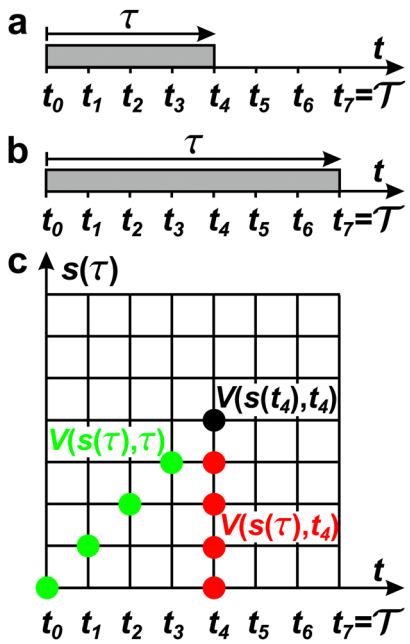

Fig. 1 (a) The time-integration limits of eqn (21) with (a) $\Gamma = t$ and (b) $\Gamma = \mathcal{T}$ depicted for the specific case of estimating $c(t_4)$ for n = 8 time-points $\{t_j\}$ [eqn (23)]. (c) Graphical illustration of the estimation of $c_w^t(t_4)$ for one walker by using the analytical solution of eqn (27), which involves the parameters A [eqn (25a)], C [eqn (25c)], and D [eqn (25d)]. The bias-potential terms for parameter C, $V(s_w(\tau_k), \tau_k)$ and for parameter D, $V(s_w(t_4), t_4)$, are depicted by green and black dots, respectively, whereas parameter A involves both $V(s_w(\tau_k), t_4)$ (red dots) and $V(s_w(\tau_k), \tau_k)$. Note that the index $0 \leq k \leq 3$ implies that τ is integrated up to t_4, as in (a).

We refer to ref. 38 for details on practical ITRE implementations within the metadynamics scope, whereas Section 3.1 presents a modified procedure implemented herein within VES, along with extensions to multiple-walker simulations.

3. Enhanced reweighting procedures

3.1 New reweighting protocols

The metadynamics-associated ITRE strategy by Giberti *et al.*[38] for estimating $c(t)$ by integrating eqn (20) over the history of $V(s, t)$ is readily generalized to multiple-walker simulations within the VES framework, which may involve N_{W} independent or cooperative walkers. Note that for a given simulation, all—independent and/or collective—walkers share the same bias potential and only differ in their bias-*correction* functions (*vide infra*). Hence, "independent walkers" should *not* be confused with "independent simulations". Moreover, the time-integration of eqn (20) may for each case be evaluated by either using t (as in ref. 38) or $\mathcal{T}$ as upper integration limit (Fig. 1a,b), which lead to time-*dependent* $[P(s, t)]$ and time-*independent* $[P(s, \mathcal{T})]$ distribution functions, respectively. Consequently, combination of both pairs of "walker" and "time-integration" options furnishes four new reweighting methods: each one is denoted by $M_{\mathcal{W}}^{\Gamma}$, where the time-integration limit is given by the superscript $\Gamma = t$ or $\Gamma = \mathcal{T}$, while the subscript $\mathcal{W}$ identifies the scenarios of either *cooperative* ($\mathcal{W} = \Sigma$) or *independent* ($\mathcal{W} = w$) walkers, where "w" is an index $w = \{1, 2, \ldots, N_{\mathrm{W}}\}$.

Each *independent* walker w associates with its "own/unique" function, $c_w^{\Gamma}(t)$, calculated by a generalized form of eqn (20), according to

$$\exp\{-\beta c_w^{\Gamma}(t)\} = \frac{\int_0^{\Gamma} \mathrm{d}\tau\, \exp\{\beta[V(s_w(\tau),\tau)-c_w^{\Gamma}(\tau)-V(s_w(\tau),t)]\}}{\int_0^{\Gamma} \mathrm{d}\tau\, \exp\{\beta[V(s_w(\tau),\tau)-c_w^{\Gamma}(\tau)]\}}, \quad (21)$$

where $s_w(\tau)$ is the CV value of walker w at time-point τ. All *cooperative* walkers, on the other hand, share the same bias-correction function, $c_{\Sigma}^{\Gamma}(t)$, which is obtained from

$$\exp\{-\beta c_{\Sigma}^{\Gamma}(t)\} = \frac{\int_0^{\Gamma} \mathrm{d}\tau \sum_{w=1}^{N_{\mathrm{W}}} \exp\{\beta[V(s_w(\tau),\tau)-c_{\Sigma}^{\Gamma}(\tau)-V(s_w(\tau),t)]\}}{\int_0^{\Gamma} \mathrm{d}\tau \sum_{w=1}^{N_{\mathrm{W}}} \exp\{\beta[V(s_w(\tau),\tau)-c_{\Sigma}^{\Gamma}(\tau)]\}}. \quad (22)$$

Eqn (21) and (22) were in practice implemented by sampling each $s_w(\tau)$ function at n discrete time-points

$$\{t_0 \equiv 0, t_1, t_2, \ldots, t_j, \ldots, t_{n-1} = \mathcal{T}\}, \quad \text{with } t_j = j\Delta\tau \quad (23)$$

with $\Delta\tau = \mathcal{T}/(n-1)$, yielding a self-consistent system of equations with the solution $\{c(t_0), c(t_1), \ldots, c(t_{n-1})\}$, as depicted schematically in Fig. 1a,b.

Because the ITRE protocol[38]—along with its generalized multiple-walker expressions given herein [eqn (21) and (22)]—compute $c(t)$ by time integration up to either t (ref. 38) or to $\mathcal{T}$, they do not explicitly assume ergodicity and are thereby less prone to acquire systematic errors that may decelerate the

 This journal is © the Owner Societies 2023

Open Access Article. Published on 03 July 2023. Downloaded on 1/21/2026 10:11:48 PM. This article is licensed under a Creative Commons Attribution 3.0 Unported Licence.

metadynamics/VES convergence. Notably, that contrasts with the M_Σ^{TP} and M_Σ^{VES} approaches of ref. 17, 36, and 37 that utilize *s*-integration and rely on the validity of eqn (16); see Section 2.3.1. Albeit their reweighting accuracy may improve by restricting the evaluation of eqn (15) to the data with $t \geq t_{min}$, the precise value of t_{min} is *a priori* unknown and must be deduced empirically.[19,36]

The reweighting evaluations herein included the entire time domain to enable continuous "convergence curves" for all methods and simulation periods $\mathcal{T}$ (Section 5), thereby offering practical assessments of M_Σ^{TP} and M_Σ^{VES} against the new time-integration-based reweighting protocols, none of which requires any $t < t_{min}$ truncation of the data set and consequently also no assumptions about the unknown limit t_{min}. This feature is a decisive advantage of reweighting by time-integration.[38]

3.2 Analytical solutions for the bias-correction function $c(t)$

Albeit the computational efforts of the reweighting stage remain truly marginal as compared with those of its underlying MD simulations and eqn (22) may be solved in $\approx$3 iterations,[38] here we provide analytical solutions for the bias-correction functions $c_\Sigma^t(t)$ and $c_w^t(t)$, whose computational costs match that of *one sole* numerical iteration cycle, thereby offering significant advantages both in terms of speed and accuracy.

To solve eqn (22) analytically, we express it according to

$$\exp\{-\beta c(t_j)\} = \frac{A + B\exp\{-\beta c(t_j)\}}{C + D\exp\{-\beta c(t_j)\}}, \quad 0 \leq j \leq n-1, \quad (24)$$

where each parameter A, B, C, and D is given by a summation over exponentiated functions evaluated at time-points $\{t_j\}$ [eqn (23)], each separated by $\Delta\tau$:

$$A = \Delta\tau \sum_{k=0}^{j-1} \sum_{w=1}^{N_W} \exp\{\beta[V(s_w(\tau_k), \tau_k) - V(s_w(\tau_k), t_j) - c(\tau_k)]\}, \quad (25a)$$

$$B = \Delta\tau N_W, \quad (25b)$$

$$C = \Delta\tau \sum_{k=0}^{j-1} \sum_{w=1}^{N_W} \exp\{\beta[V(s_w(\tau_k), \tau_k) - c(\tau_k)]\}, \quad (25c)$$

$$D = \Delta\tau \sum_{w=1}^{N_W} \exp\{\beta V(s_w(t_j), t_j)\}. \quad (25d)$$

Fig. 1c illustrates the various time-dependent bias-potential components $[V(s_w(\tau_k), t_j)]$ of eqn (25) for one walker and t_j value. Here, the C and D parameters depend only on the values $V(s_w(\tau_k), \tau_k)$ (green dots) and $V(s_w(t_j), t_j)$ (black dot), respectively, whereas A involves both $V(s_w(\tau_k), t_j)$ (red dots) and $V(s_w(\tau_k), \tau_k)$.

By identifying $x_j \equiv \exp\{-\beta c(t_j)\}$, eqn (24) may be represented as

$$Dx_j^2 + (C - B)x_j - A = 0, \quad 0 \leq j \leq n-1, \quad (26)$$

which may be solved analytically:

$$c(t_j) = -\beta^{-1} \ln\left\{y + \sqrt{y^2 + A/D}\right\}, \quad \text{with } y = (B - C)/(2D). \quad (27)$$

Note that $A = C = 0$ at $t_0 = 0$, which in the absence of a bias potential $[V(s_w(t_0), t_0) = 0]$ implies that $B = D$ and $c(t_0) = 0$. For each consecutive time-point t_j ($j = 0, 1, \ldots, n-1$), eqn (25) are evaluated, whereupon $c(t_j)$ is determined from eqn (27).

Notably, eqn (27) applies to calculations of $c(t)$ for the practically most relevant scenario of cooperative walkers, whereas that for independent walkers follows trivially because each of the sums A–D in eqn (25) collapses into *one sole* term for each walker w. These analytical solutions of $c_W^t(t)$ were employed in all computations presented below.

4. Computational methods

4.1 General simulation conditions

All atomistic MD simulations involved *NVT* ensembles at $T = 37$ °C, utilizing the GROMACS v2018.1 platform.[59] The equations of motion were integrated in steps of 0.9 fs by using the velocity Verlet integrator.[55] The Coulomb interactions were calculated with a smoothed particle–mesh Ewald summation[60] of order four and a tolerance of 10^{-5}, using a Fourier spacing of 0.12 and a switch distance of 1.2 nm, while the van der Waals interactions were truncated at 1.2 nm. The temperature was controlled by the velocity rescale thermostat[61] with a 1.0 ps time constant.

The well-tempered VES simulations[17–19] employed the PLUMED2.4 software.[62] To enhance the configurational sampling, a well-tempered target distribution with bias factor $\gamma = 5$ was employed along with the CV. The time-dependent bias potential, $V(s, t)$, was expanded out to order $N_F = 6$ in the CV (eqn (14)). The well-tempered target distribution $P_V(s, t) = \exp\{\beta V(s, t)/(\gamma - 1)\}$ and the $\{\alpha_k(t)\}$ coefficients were calculated iteratively during the simulation by using the averaged-stochastic-gradient descent algorithm[63] with a step size of $\mu = 1.0$ to minimize the variational functional eqn (12) by the procedures described in ref. 17 and 63. The time integration spans the interval $\Delta\tau$ between each bias-potential update.[17] To minimize numerical errors, the Fourier coefficients $\{\alpha_k(t)\}$ were updated every $\Delta\tau = 0.9$ ps and then stored at each time-point, while $P_V(s, t)$ was updated every 0.45 ns.

The accuracy of the bias-potential evaluation was improved by sampling different CV domains by employing N_W walkers, each operating within an independently generated system and starting from different configurations to ensure that they sample different MD trajectories.

4.2 Alanine dipeptide simulations

One *N*-acetyl-L-alanine methylamide molecule—henceforth referred to as "alanine dipeptide" (Fig. 2)—was simulated in vacuum by using the CHARMM36/CMAP all-atom force field (July 2017).[64] The volume of the cubic cell was kept constant at $V = 36.7$ nm^3 to avoid undesirable boundary-condition effects.

Open Access Article. Published on 03 July 2023. Downloaded on 1/21/2026 10:11:48 PM.
This article is licensed under a Creative Commons Attribution 3.0 Unported Licence.

The simulations were performed with two distinct CVs represented by either torsion angle $s = \phi$ or $s = \psi$ (Fig. 2), as well as with ensembles of $N_W = \{4, 8, 16, 64\}$ cooperative and independent walkers. As described further in Section 5.1, every simulated $\{s, N_W\}$ combination was reweighted by each novel $\{M_\Sigma^t, M_\Sigma^\mathcal{T}, M_w^t, M_w^\mathcal{T}\}$ protocol along with M_Σ^{TP} (ref. 36) and M_Σ^{VES} (ref. 17 and 37), by evaluating ΔF between two metastable molecular conformations for increasing $\mathcal{T}$ (see Section 5.1).

The convergence of each reweighting method was assessed from $N_{sim} = \{16, 16, 8, 6\}$ independent but nominally identical simulations for the respective walker ensembles with $N_W = \{4, 8, 16, 64\}$ by calculating the root-mean-square (rms) deviation of $\Delta F \equiv \Delta F(\mathcal{T})$ to the fully converged reference value $\Delta F_{ref} = 6.80$ kJ mol^{-1}, *i.e.*, we evaluated the entity $\mathrm{rms}(\Delta F(\mathcal{T}) - \Delta F_{ref})$. ΔF_{ref} was determined from three independent VES/MD simulations that utilized both CVs, $s = \{\phi, \psi\}$, for a long simulation period of $\mathcal{T}$=100 ns (using one walker). Moreoever, because the bias-potential $V(s, t)$ converged well within 20 ns, employing the standard VES reweighting protocol[17–19] for $t > 20$ ns yielded the same value of $\Delta F_{ref} = 6.80$ kJ mol^{-1} for all three simulations. Note that all reweighting methods converge to the same result (see Section 5.1). The initial configuration of each walker of the subsequent N_{sim} simulations constituted a randomly selected frame for $t > 20$ ns of the fully converged 100 ns MD simulations.

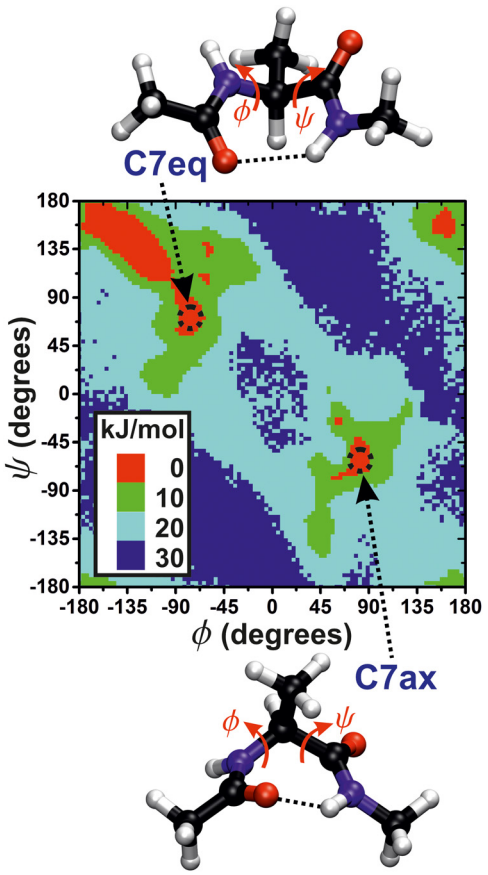

Fig. 2 Illustration of the two "C7eq" and "C7ax" molecular conformations of *N*-acetyl-L-alanine methylamide ("alanine dipeptide") with the two torsion angles ϕ and ψ indicated, along with the free-energy surface.

The variance among the $\mathrm{rms}(\Delta F(\mathcal{T}) - \Delta F_{ref})$ results of the N_{sim} simulations was determined by the Jackknife method[65] according to

$$\sigma^2[\mathrm{rms}(\Delta F - \Delta F_{ref})] = (N_{sim} - 1)^{-1} \sum_{k=1}^{N_{sim}} \{y_k - \mathrm{rms}(\Delta F - \Delta F_{ref})\}^2, \quad (28)$$

$$y_k^2 = (N_{sim} - 1)^{-1} \sum_{j \neq k}^{N_{sim}} (\Delta F_j - \Delta F_{ref})^2. \quad (29)$$

4.3 Analytical potential-model simulations

We simulated an *NVT* ensemble of 1000 water molecules with the force field of ref. 66 in a cubic box of equal axis lengths $l_x = l_y = l_z = 3.1$ nm. An internal reference point was obtained by restricting the position of one molecule at origo by an harmonic potential with a large force constant (κ = 250 kJ mol^{-1}). The center-of-mass of *one* other water molecule, referred to as "A", was restricted at $y = 1.3$ nm. The intermolecular separation was around $l_y/2$, which ensured that the two molecules are further apart than the cutoff distance of 1.2 nm for all Coulomb and van der Waals interactions. The position of molecule A along the x direction was subjected to the periodic free-energy function

$$F(x)/(\mathrm{kJ\ mol^{-1}}) = 5\cos\{6x2\pi/l_x\}, \quad (30)$$

which possesses six local energy minima, all separated by a barrier of 10 kJ mol^{-1}.

The system was simulated with the collective variable $s = 2\pi x/l_x$ (which is the optimal choice), $N_W = 6$, and $\gamma = 5$, which ensures the asymptotic relationship $V(x) = -(1 - \gamma^{-1})F(x) = -(4/5)F(x)$:

$$V(x)/(\mathrm{kJ\ mol^{-1}}) = -4\cos\{6x2\pi/l_x\}. \quad (31)$$

The bias potential was applied to molecule A along the x direction, whereas no other direction or molecule was biased. Hence, all walkers shared the same energy minimum at $x \approx 0.8$ nm (see Section 5.2), yet at slightly different positions to ensure that each follows a unique trajectory. The results presented below are averages over 32 independent but nominally identical simulations.

5. Results and discussion

5.1 Alanine dipeptide conformations

Owing to its extensive use in developments of metadynamics and other ES methods,[12,14,17,19,26,27,36,37,54] the alanine dipeptide molecule in vacuum was selected for benchmarking the new $\{M_\Sigma^t, M_\Sigma^\mathcal{T}, M_w^t, M_w^\mathcal{T}\}$ reweighting options, which are contrasted with the already established state-of-the-art M_Σ^{TP} (ref. 36) and M_Σ^{VES} (ref. 17 and 37) schemes. The convergence offered by each protocol was evaluated for (i) increasing simulation time ($\mathcal{T}$), when (ii) using either of the torsion angle ϕ or ψ as CV, and (iii) variable-sized walker ensembles with $N_W = \{4, 8, 16, 64\}$.

 This journal is © the Owner Societies 2023

Open Access Article. Published on 03 July 2023. Downloaded on 1/21/2026 10:11:48 PM. This article is licensed under a Creative Commons Attribution 3.0 Unported Licence.

Here, we assessed the convergence of the free-energy difference between two metastable molecular conformations that form a seven-atom membered cyclic structure, labeled "C7", and stabilized by an internal hydrogen bond. These two conformations are shown in Fig. 2, along with the $F(s)$ contours plotted against ϕ and ψ. The three methyl groups of the molecule may assume either equatorial (C7eq) or axial (C7ax) orientations relative to the ring, respectively. We assessed the convergence performance of each $\{M_\Sigma^t, M_\Sigma^\mathcal{T}, M_w^t, M_w^\mathcal{T}, M_\Sigma^{\mathrm{TP}}, M_\Sigma^{\mathrm{VES}}\}$ reweighting procedure *via* the free-energy difference

$$\Delta F(\mathcal{T}) = -\beta^{-1} \ln\left\{\frac{P(\mathrm{C7ax})}{P(\mathrm{C7eq})}\right\} \tag{32}$$

between two torsion-angle domains $\mathcal{D} = \{\phi, \psi: \sqrt{(\phi-\phi_\mathcal{D}^0)^2 + (\psi-\psi_\mathcal{D}^0)^2} < 10^\circ\}$ centered at $\Omega(\mathcal{D}^0) \equiv \{\phi_\mathcal{D}^0, \psi_\mathcal{D}^0\}$, with $\Omega(\mathrm{C7eq}^0) = \{-81^\circ, 71^\circ\}$ and $\Omega(\mathrm{C7ax}^0) = \{74^\circ, -67^\circ\}$, respectively. The probability $P(\mathcal{D})$ of domain $\mathcal{D}$ is

$$P(\mathcal{D}) = \frac{\int_0^\mathcal{T} \mathrm{d}t \sum_{w=1}^{N_\mathrm{W}} \chi_\mathcal{D}(\Omega_w(t)) \exp\{\beta[V(s_w(t),t) - c(t)]\}}{\int_0^\mathcal{T} \mathrm{d}t \sum_{w=1}^{N_\mathrm{W}} \exp\{\beta[V(s_w(t),t) - c(t)]\}}, \tag{33}$$

where the function $\chi_\mathcal{D}(\Omega_w(t))$ is unity throughout $\mathcal{D}$ and zero otherwise.

5.1.1 Role of walkers and choice of collective variable for convergence. For each collective variable $s = \phi$ and $s = \psi$, Fig. 3 plots the convergence function, $\mathrm{rms}(\Delta F - \Delta F_\mathrm{ref})$, for increasing MD simulation intervals $\mathcal{T}$ and walker ensembles with 4 to 64 members. All reweighting schemes converge markedly more rapidly for the simulations with $s = \phi$ than those for $s = \psi$. Hence, $s = \phi$ is a "good" choice of CV because it manifests pronounced transition-state barriers between the energy minima (Fig. 2), which are readily compensated for by the bias potential $V(\phi, t)$, whereas the selection $s = \psi$ leads to a "hystereses" behavior that results in slow convergence.[14,19]

These features are more transparent in the corresponding plots of Fig. 4 which are zoomed around the "near-convergence" domain (dotted rectangles in Fig. 3). Indeed, Fig. 4b and Table 1 reveals that for simulations with $s = \psi$ and $N_\mathrm{W} = 4$, only the data reweighted by M_Σ^t, M_Σ^{TP} and M_Σ^{VES} reach below the convergence threshold (horizontal red dotted lines in Fig. 3 and 4) within our longest evaluated value of $\mathcal{T} = 20$ ns, requiring the corresponding simulation periods of 13.7 ns, 14.0 ns, and 19.4 ns, respectively. However, while these *rms* results over $N_\mathrm{sim} = 16$ independent simulations meet the convergence criterion, *only* the M_Σ^t and M_Σ^{TP} reweighting schemes offer convergence for all simulations (upon omission of obvious outliers; see Table 1), both requiring $\mathcal{T} \approx 19$ ns. Fig. S1 and S2 (ESI†) show the convergence curves with $\pm\sigma$ spreads among the N_sim simulations of each reweighting scheme.

The overall most rapid $\mathrm{rms}(\Delta F - \Delta F_\mathrm{ref})$ convergence resulted when employing (moderately) large walker ensembles (Fig. 3c–h and 4c–h). This property is most evident for the simulations with the "unfavorable" CV ψ, where all walker ensembles with $N_\mathrm{W} \geq 8$ secured proper convergence within 20 ns for all reweighting schemes but M_w^t. Moreover, regardless of the precise choice of CV, Fig. 3 and 4 reveal that *cooperative* walkers (*i.e.*, M_Σ^t and $M_\Sigma^\mathcal{T}$) are markedly more favorable than independent ones (*i.e.*, M_w^t and $M_w^\mathcal{T}$). Their advantage emphasizes progressively for increasing N_W, which reflects the enhanced statistics provided by sets of cooperative walkers for improved $c(t)$ estimates.

We remind that Fig. 3 and 4 employ a logarithmic time scale and that the differences in convergence merits are substantial between the favorable $\{M_\Sigma^t, M_\Sigma^\mathcal{T}\}$ and worse $\{M_w^t, M_w^\mathcal{T}\}$ pairs of reweighting protocols. For the herein most favorable $\{s = \phi, N_\mathrm{W} = 64\}$ simulation scenario, the reweighting method with collective walkers $(M_\Sigma^\mathcal{T})$ required $\mathcal{T} = 200$ ps to attain "sufficient" convergence of $\mathrm{rms}(\Delta F - \Delta F_\mathrm{ref})$, whereas its counterpart with independent walkers $(M_w^\mathcal{T})$ demanded 670 ps (Table 1). For the $N_\mathrm{W} = 64$ walker ensemble with the less favorable CV $s = \psi$, the $M_\Sigma^\mathcal{T}$ scheme required 290 ps for convergence, whereas $M_w^\mathcal{T}$ necessitated 7.34 ns (Fig. 4h). The differences in convergence properties among the M_Σ^t and M_w^t schemes are even larger (Table 1): M_Σ^t offers very similar convergence as $M_\Sigma^\mathcal{T}$ for $N_\mathrm{W} = 64$ regardless of the choice of s. In contrast, the M_w^t counterpart does not converge within 20 ns for the "difficult" $s = \psi$ case, irrespective of the walker-ensemble size, while it takes 6–29 times longer to converge (relative to M_Σ^t) for all $s = \phi$ scenarios with $N_\mathrm{W} \geq 8$. Besides the expected finding that larger walker ensembles accelerate the convergence relative to smaller ones, we conclude that cooperative walkers are preferred to independent ones.

5.1.2 Role of time-integration limit for convergence. Because the M_Σ^{TP} and M_Σ^{VES} reweighting schemes utilize CV integration, we here only contrast the novel $\{M_\Sigma^t, M_\Sigma^\mathcal{T}, M_w^t, M_w^\mathcal{T}\}$ protocols generalized from the ITRE procedure. For the smallest walker ensembles with $N_\mathrm{W} = 4$ of Fig. 3a,b and 4a,b, significant differences are observed for the $\mathrm{rms}(\Delta F - \Delta F_\mathrm{ref})$ results between the protocols employing $\Gamma = t$ relative to $\Gamma = \mathcal{T}$ for *both* cooperative and independent walker ensembles, where the integration limit t is favorable throughout. Here, the M_Σ^t reweighting scheme outperforms any other time-integration-based reweighting option.

For larger ensembles with at least 8 *independent* walkers, the results of Fig. 3c–h and 4c–h reveal that the $M_w^\mathcal{T}$ protocol with integration limit $\mathcal{T}$ offers a substantially faster reweighting convergence than its M_w^t sister scheme. Nontetheless, $M_w^\mathcal{T}$, and (in particular) M_w^t, remain overall inferior to their cooperative-walker based $M_\Sigma^\mathcal{T}$ and M_Σ^t counterparts (Section 5.1.1). The latter procedures exhibit nearly equal reweighting performances both far from (Fig. 3) and near/at (Fig. 4) convergence, regardless of the precise simulation period and the number of walkers. We attribute the property of a largely immaterial choice of integration limit $\Gamma = t$ (M_Σ^t) or $\Gamma = \mathcal{T}$ $(M_\Sigma^\mathcal{T})$ for the ensembles of cooperative walkers to their accompanying enhanced sampling of the CV domain, thereby also naturally reducing the differences between averages over time or over CVs.

Open Access Article. Published on 03 July 2023. Downloaded on 1/21/2026 10:11:48 PM.
This article is licensed under a Creative Commons Attribution 3.0 Unported Licence.

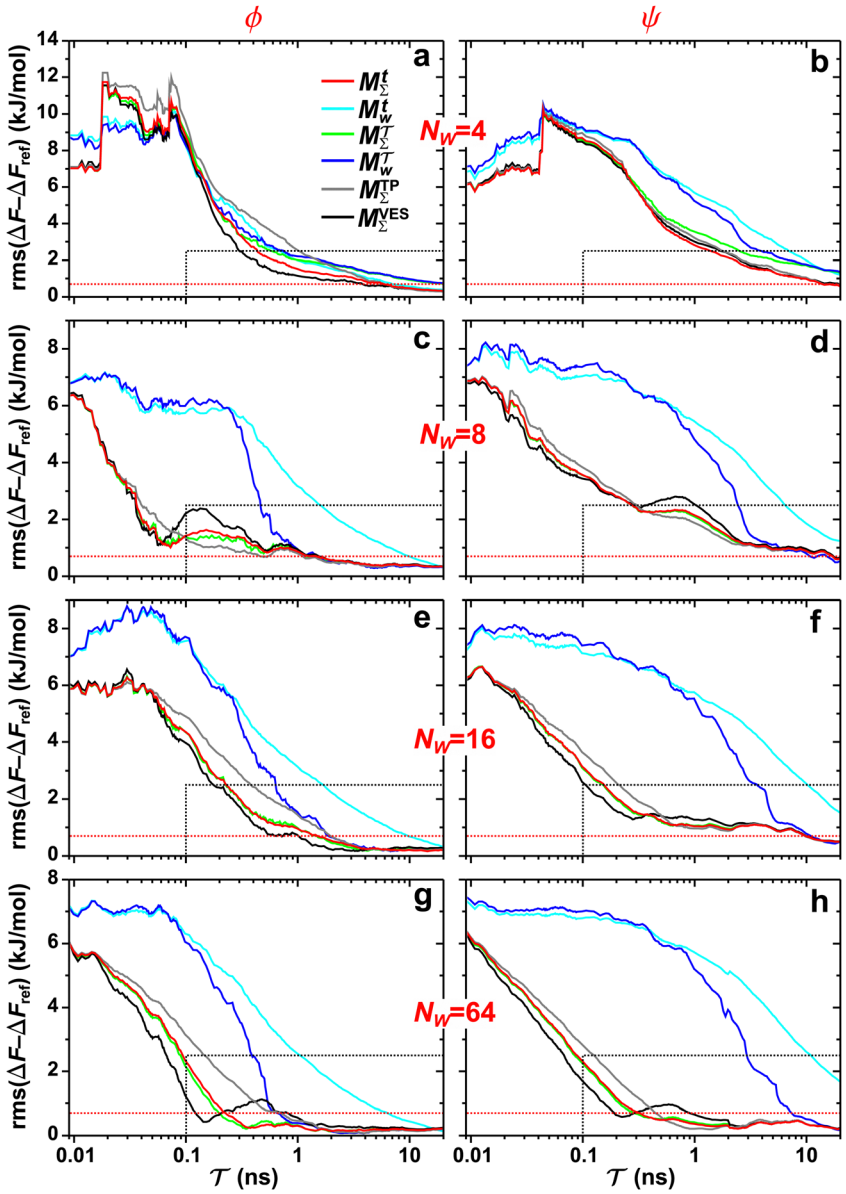

Fig. 3 Plots of rms$(\Delta F(\mathcal{T}) - \Delta F_{ref})$ [eqn (32)] against the simulation interval $\mathcal{T}$ (log scale) for the herein proposed $\{M_\Sigma^t, M_w^t, M_\Sigma^\mathcal{T}, M_w^\mathcal{T}\}$ reweighting protocols, along with those by Tiwary and Parrinello[36] (M_Σ^{TP}) and that of Schäfer and Settanni,[37] which is identical to the original VES reweighting[17,18] (M_Σ^{VES}). The VES/MD simulations employed ensembles of (a, b) 4, (c, d) 8, (e, f) 16, and (g, h) 64 walkers along with collective variables of $s = \phi$ (left panel) and $s = \psi$ (right panel). Each dotted rectangle and horizontal red dotted line in (a)–(d) marks the respective regions of "near" and "sufficient" convergence to the correct reference energy value ΔF_{ref} = 6.80 kJ mol^{-1}. The relative performances of the various reweighting protocols in the near-convergence regimes are more transparent in the zoomed plots shown in Fig. 4. Note that the vertical plot ranges varies among the rows of graphs and that the converge accelerate consistently for increasing walker ensembles. Each rms$(\Delta F - \Delta F_{ref})$ curve resulted from (a)–(d) 16, (e, f) 8, and (g, h) 6 independent simulations; Fig. S1 and S2 (ESI†) plot the data uncertainties.

When all results of Fig. 3 and 4 are taken together for the $\{M_\Sigma^t, M_\Sigma^\mathcal{T}, M_w^t, M_w^\mathcal{T}\}$ reweighting procedures evaluated for different CVs, walker-ensemble types and sizes, the overall best and near-equal performances are observed for the cooperative-walkers based M_Σ^t and $M_\Sigma^\mathcal{T}$ protocols. Yet we recommend using the M_Σ^t scheme due to its markedly faster convergence *also* for very small walker ensembles (Fig. 3a,b and 4a,b), along with much more rapid reweighting calculations (Table S1, ESI†).

5.1.3 Relative reweighting merits. Here, we focus on contrasting the two best time-integration protocols, M_Σ^t and $M_\Sigma^\mathcal{T}$, with the *s*-integration based M_Σ^{TP} and M_Σ^{VES} schemes. Relative to the M_Σ^{TP} protocol introduced by Tiwary and Parrinello[36], Schäfer and Settanni[37] highlighted primarily two advantages with their balanced-exponential reweighting method: (i) a faster convergence for "short" simulation periods, and (ii) lower reweighted-observable uncertainties/variabilities. At least within the scope

 This journal is © the Owner Societies 2023

Open Access Article. Published on 03 July 2023. Downloaded on 1/21/2026 10:11:48 PM.
This article is licensed under a Creative Commons Attribution 3.0 Unported Licence.

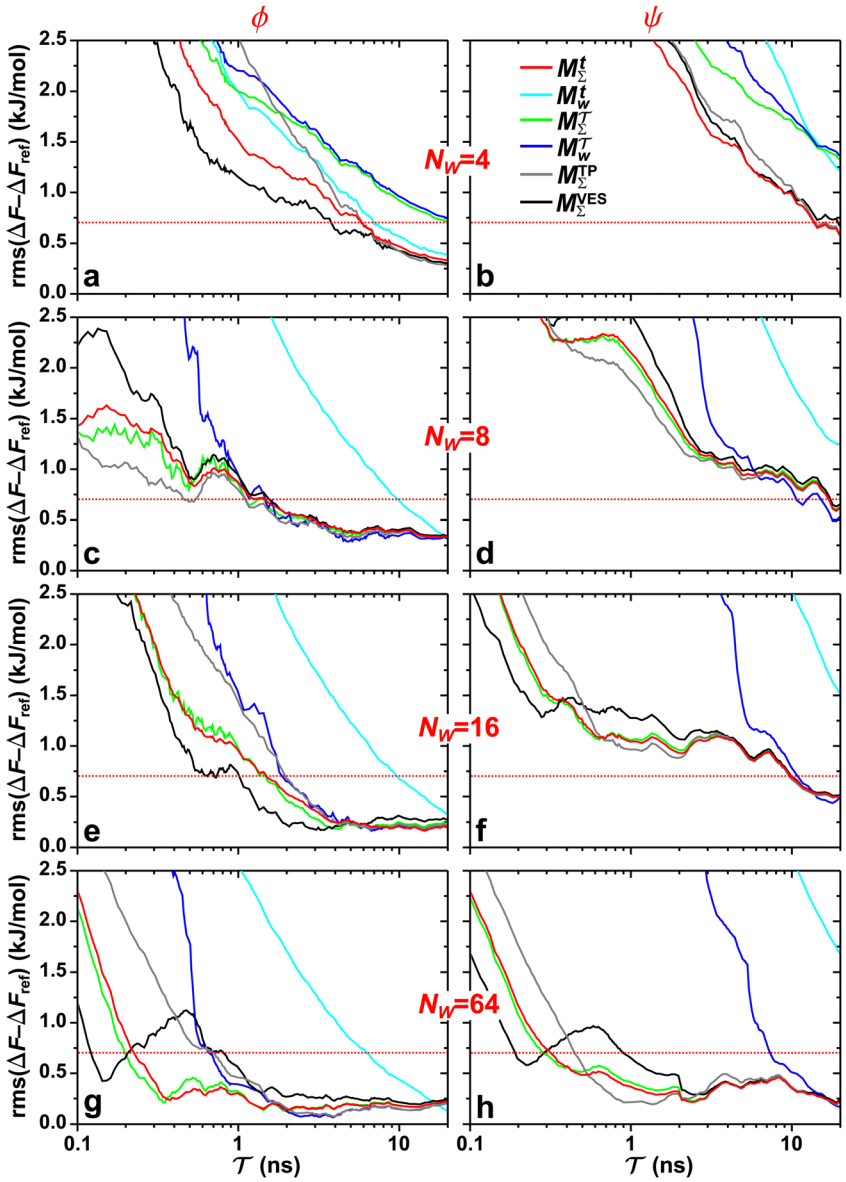

Fig. 4 Zoomed convergence plots of the near-convergence region shown by dotted rectangles in Fig. 3.

of VES—for which the BE and VES reweighting procedures become identical (M_Σ^{VES})—the second claim is generally neither born out by our assessments for the alanine dipeptide (*vide infra*) nor for the case examined in Section 5.2. The perhaps more important claim (i) of better reweighting convergence properties for short MD simulation periods, however, appears to depend significantly on the particular choice of CV(s) and walker-ensemble size: for relatively large number of walkers $N_{\mathrm{W}} = \{16, 64\}$, the M_Σ^{VES} protocol indeed offers more rapid convergence regardless of $s = \{\phi, \psi\}$ (Fig. 3). Yet, these improvements are typically only pronounced in regimes *too far* from a reasonable convergence demand. Throughout both regimes of "near" and "sufficient" convergence, the VES/BE reweighting consistently *only* outperformed all other methods for the cases of $s = \phi$ with $N_{\mathrm{W}} = \{4, 16\}$; see Fig. 3a,e and 4a,e.

A lack of reliability appears to be the main deficiency of the original VES reweighting (Fig. 3–5, Fig. S1, and S2, ESI†): for the largest-walker simulations close to convergence (Fig. 4g,h), the highly oscillatory rms($\Delta F - \Delta F_{\mathrm{ref}}$) curve of M_Σ^{VES} renders it inferior relative to its primary M_Σ^t, $M_\Sigma^{\mathcal{T}}$, and M_Σ^{TP} competitors. The required simulation periods to attain convergence ($\mathcal{T}_{\mathrm{conv}}$) among the protocols for $\{s = \phi, N_{\mathrm{W}} = 64\}$ increase according to $M_\Sigma^t \approx M_\Sigma^{\mathcal{T}} < M_w^{\mathcal{T}} < M_\Sigma^{\mathrm{TP}} < M_\Sigma^{\mathrm{VES}} \ll M_w^t$ (Table 1), while the case of $s = \psi$ only differs in that $\mathcal{T}_{\mathrm{conv}}(M_w^{\mathcal{T}}) \approx \mathcal{T}_{\mathrm{conv}}(M_\Sigma^{\mathrm{TP}})$. The 8-walker ensemble evaluations for $s = \phi$ shown in Fig. 4c reveal a similar trend, except that now the M_Σ^{TP} protocol performs overall best, both to reach convergence and within the "near convergence" regime (<1 ns). Hence, as for the VES/BE reweighting, the Tiwary and Parrinello scheme manifests an uneven performance among the simulations in Fig. 3 and 4, in

Open Access Article. Published on 03 July 2023. Downloaded on 1/21/2026 10:11:48 PM.
This article is licensed under a Creative Commons Attribution 3.0 Unported Licence.

Table 1 Simulation time $\mathcal{T}_{\rm conv}$ (in ns) to reach convergence[a]

Alanine dipeptide

$s-N_{\rm W}$[b]	$N_{\rm sim}$	M_{Σ}^{t}	$M_{\Sigma}^{\mathcal{T}}$	M_{w}^{t}	$M_{w}^{\mathcal{T}}$	$M_{\Sigma}^{\rm TP}$	$M_{\Sigma}^{\rm VES}$
$\phi-4$	16	5.78(10.7[1])	20.0(−)	6.93(14.5[2])	−(−)	5.89(11.8[1])	3.78(11.5[1])
$\phi-8$	16	1.45(4.13)	1.45(9.36)	9.87(13.2[2])	1.45(7.65)	1.10(7.98)	1.57(9.72)
$\phi-16$	8	1.47(1.67[1])	1.46(2.27[1])	9.59(12.0[1])	1.89(2.17[1])	1.97(2.31[1])	1.01(1.75[1])
$\phi-64$	6	0.22(0.43)	0.20(0.530)	6.30(7.95)	0.66(1.08)	0.71(1.08)	0.81(1.03)
$\psi-4$	16	13.7(18.6[3])	−(−)	−(−)	−(−)	14.0(19.2[3])	19.4(−)
$\psi-8$	16	17.0(17.6[2])	17.1(18.6[2])	−(−)	15.2(18.6[2])	17.0(18.6[2])	17.4(18.6[2])
$\psi-16$	8	9.8(10.0[1])	9.8(10.4[1])	−(−)	10.9(11.7[2])	9.64(10.4[2])	9.96(10.7[2])
$\psi-64$	6	0.32(2.66)	0.29(2.82)	−(−)	7.34(9.53[1])	0.45(9.21)	0.90(9.81)

Analytical potential

$N_{\rm s}$[c]	$N_{\rm sim}$	M_{Σ}^{t}	$M_{\Sigma}^{\mathcal{T}}$	$M_{\Sigma}^{\rm TP}$	$M_{\Sigma}^{\rm VES}$
6	32	0.150(0.237)	0.170(0.269)	0.240(0.560)	0.700(1.29)
48	32	0.210(0.285)	0.220(0.503)	0.270(0.578)	0.770(1.38)

[a] The VES/MD simulation time required for reaching convergence ($\mathcal{T}_{\rm conv}$) of either rms($\Delta F-\Delta F_{\rm ref}$) (alanine dipeptide; Fig. 3 and 4) or $D_{\rm KL}$ (analytical potential model; Fig. 6b,c) when employing the given reweighting protocol. The values within parentheses represent the corresponding $\mathcal{T}_{\rm conv}$ values required for all of the $N_{\rm sim}$ independent simulations to converge; each superscript marks the number of outlier data-curves that were omitted to give the as-stated result. [b] Collective variable and size of walker ensemble. [c] Number of bins employed to evaluate eqn (35) with $N_{\rm s}=6$ (Fig. 6b) or $N_{\rm s}=48$ (Fig. 6c).

contrast to the two best time-integration-based protocols (*i.e.*, M_{Σ}^{t} and $M_{\Sigma}^{\mathcal{T}}$), whose convergence improve monotonically for increasing walker ensembles (Table 1). The uneven performance of both *s*-integration-based reweighting protocols—which is most pronounced for VES/BE—presumably originates from the herein strict evaluations that involved reweighting based on the entire simulated time domain; this is examined further in Section 5.2.

Concerning the simulation periods for reaching convergence of rms($\Delta F-\Delta F_{\rm ref}$) for the altogether eight $\{s, N_{\rm W}\}$ combinations (Table 1), the TP and VES/BE protocols offer the most rapid convergence in two cases each, whereas the $M_{\Sigma}^{t}/M_{\Sigma}^{\mathcal{T}}$ counterparts accomplishes that in three cases, where we remind that the $M_{\Sigma}^{\mathcal{T}}$ and M_{Σ}^{t} schemes reveal essentially equal $\mathcal{T}_{\rm conv}$ values throughout, except for the smallest walker ensembles of each $s=\{\phi,\psi\}$ angle (Section 5.1.1). Moreoever, whenever the $M_{\Sigma}^{t}/M_{\Sigma}^{\mathcal{T}}$ methods do not offer the most rapid convergence, their performances remain close to the best method. Notably, for the much less forgiving criterion that *all* $N_{\rm sim}$ simulations of each method must converge, however, the M_{Σ}^{t} procedure perform best *throughout* the eight evaluated $\{s, N_{\rm W}\}$ scenarios (Table 1); yet, the difference to the second-best reweighting scheme is often marginal.

The high precision and reliability of the M_{Σ}^{t} protocol is gratifying when considering the linear scaling of the total simulation time against $N_{\rm sim}$, thereby in practice requiring a reasonable small number of independent simulations to accomplish an accurate average/rms value of $\langle O(R)\rangle$. Hence, it is desirable that the reweighting method yields the lowest possible spread (variance) around the *a priori* unknown average/rms result, such that one sole simulation and its subsequent observable-reweighting may be expected to approximate well the fully converged value obtained from a (very) large number of $N_{\rm sim}$ independent simulations.

Fig. 5 plots the variance—σ^2[rms($\Delta F-\Delta F_{\rm ref}$)] calculated from eqn (28)—observed from each reweighting protocol of Fig. 3 for increasing $\mathcal{T}$ among the $N_{\rm s}$ simulations, employing $N_{\rm sim}=\{16, 16, 8, 6\}$ for the respective walker ensembles with $N_{\rm W}=\{4, 8, 16, 64\}$. The M_{Σ}^{t}, $M_{\Sigma}^{\mathcal{T}}$ and $M_{\Sigma}^{\rm TP}$ reweighting schemes offer the overall lowest variances, all of which are similar. As for the higher convergence rate of the M_{Σ}^{t} method relative to $M_{\Sigma}^{\mathcal{T}}$ for both $s=\{\phi,\psi\}$ with $N_{\rm W}=4$ (Fig. 3a,b and 4a,b), it also features *lower* data spreads. The VES/BE protocol manifests irregular variances, which typically remain larger than those of the three best reweighting schemes for the evaluated $\{s, N_{\rm W}\}$ cases (Fig. 5). Also along the observations for the rms($\Delta F-\Delta F_{\rm ref}$) convergence in Section 5.1.1, the variances of the two M_{w}^{t} and $M_{w}^{\mathcal{T}}$ methods with independent walkers are inferior relative to their collective-walker counterparts. In particular, surprisingly high variances are observed at long simulation periods for the $M_{w}^{\mathcal{T}}$ scheme (Fig. 5), for which we have no satisfactory explanation.

5.2 Entropy assessments of an analytical free-energy model

The evaluations of the four M_{Σ}^{t}, $M_{\Sigma}^{\mathcal{T}}$, M_{w}^{t}, and $M_{w}^{\mathcal{T}}$ protocols for the alanine dipeptide suggested that simulations with reasonably large ensembles ($N_{\rm W}>4$) of *cooperative* walkers are preferable for obtaining the most accurate results, with the M_{Σ}^{t} reweighting scheme offering the overall most favorable results (Fig. 3–5 and Table 1). Our second benchmarking scenario of liquid water with an artificial free-energy perturbation [eqn (30)] applied to one molecule employs an optimal CV, $s=2\pi x/l_x$ (Section 4.3), along with a modest walker ensemble of $N_{\rm W}=6$. Consequently, we focussed on comparing the cooperative-walker based M_{Σ}^{t} and $M_{\Sigma}^{\mathcal{T}}$ protocols (which are expected to consistently gain merits relative to their M_{w}^{t}, and $M_{w}^{\mathcal{T}}$ counterparts for increasing $N_{\rm W}$) with the

 This journal is © the Owner Societies 2023

Open Access Article. Published on 03 July 2023. Downloaded on 1/21/2026 10:11:48 PM.
This article is licensed under a Creative Commons Attribution 3.0 Unported Licence.

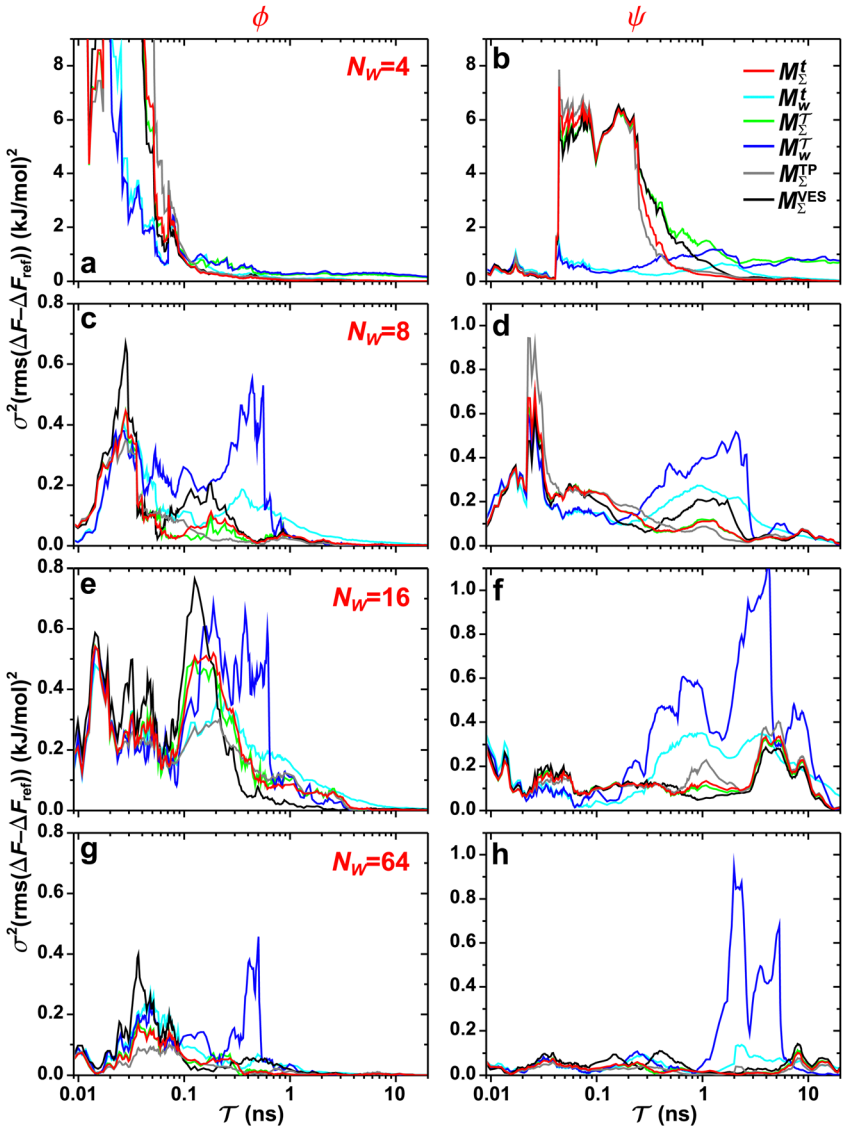

Fig. 5 The variance, $\sigma^2[\mathrm{rms}(\Delta F - \Delta F_{\mathrm{ref}})]$; eqn (28), plotted against the simulation period of each evaluated reweighting protocol of Fig. 3. Note the different vertical scales in the (a and b) plots relative to those of (c, e, g), and (d, h, f).

CV-integration associated M_Σ^{TP} (ref. 36) and M_Σ^{VES} (ref. 17 and 37) reweighting procedures.

The present problem-design with an *a priori* known $F(x)$ function acting on one water molecule along x, implies that a converged VES/MD simulation should reproduce the periodic free-energy and bias-potential functions of eqn (30) and (31), respectively. Fig. 6a plots $F(x)$ with its six local energy minima $\{\mathcal{D}_k\}$ indicated, along with the corrected bias-potential functions estimated from the M_Σ^t protocol for the simulation periods of $\mathcal{T} = 10\,\mathrm{ps}$ and 1.0 ns. Because all walkers were initially confined to the $\mathcal{D}_2$ domain centered at x = 0.8 nm [*i.e.*, $P(\mathcal{D}_2) = 1$], this population remains, as expected, strongly favored for the very short $\mathcal{T} = 10\,\mathrm{ps}$ simulation interval. In the limits of very short and long simulation periods $\mathcal{T}$, all examined reweighting protocols $\{M_\Sigma^t, M_\Sigma^\mathcal{T}, M_\Sigma^{\mathrm{TP}}, M_\Sigma^{\mathrm{VES}}\}$ yield identical results to that shown for M_Σ^t with $\mathcal{T} = 1.0\,\mathrm{ns}$ in Fig. 6a.

The convergence of each reweighting protocol was monitored *via* the estimated relative entropy, which was assessed by calculating the Kullback–Leibler divergence (D_{KL})[26,67] between the reweighted distribution and $P_{\mathrm{ref}}(s) = \exp\{-\beta F(s)\}/\int \mathrm{d}s\, \exp\{-\beta F(s)\}$:

$$D_{\mathrm{KL}} = \int \mathrm{d}s\, P(s)\, \ln\{P(s)/P_{\mathrm{ref}}(s)\}. \qquad (34)$$

Eqn (34) was in practice evaluated by a discretization into N_s bins according to

$$D_{\mathrm{KL}} = \sum_{k=1}^{N_s} P(\mathcal{D}_k)\, \ln\{P(\mathcal{D}_k)/P_{\mathrm{ref}}(\mathcal{D}_k)\}. \qquad (35)$$

A properly converged VES/MD simulation should reproduce the known reference distribution, which for the most straightforward choice of N_s = 6 becomes $P_{\mathrm{ref}}(\mathcal{D}_k) = 1/6$, meaning that all walkers distribute evenly among the six $F(x)$ minima (Fig. 6a).

Open Access Article. Published on 03 July 2023. Downloaded on 1/21/2026 10:11:48 PM.
This article is licensed under a Creative Commons Attribution 3.0 Unported Licence.

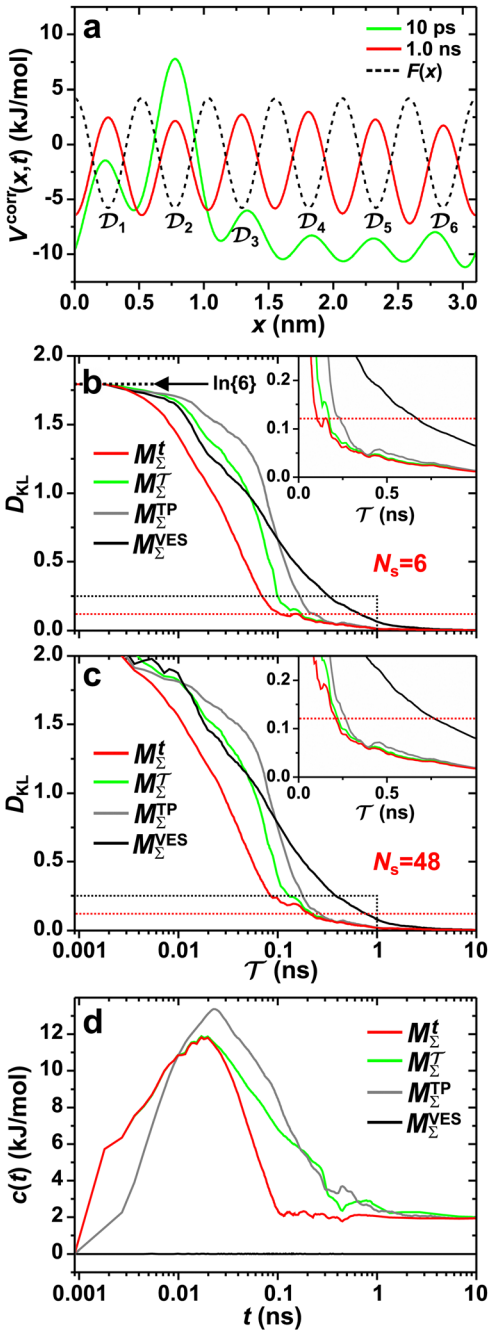

Fig. 6 (a) Corrected bias potential, $V^{corr}(x, t) = V(x, t) - c(t)$, obtained from the M_Σ^t protocol for short (green trace) and long (red trace) simulation intervals $\mathcal{T}$=10 ps and $\mathcal{T}$=1.0 ns, respectively. The dotted curve represents the applied free-energy function $F(x)$ (eqn (30)), whose six minima $\{\mathcal{D}_k\}$ are indicated beneath. (b) Convergence of the Kullback–Leibler divergence [D_{KL}; eqn (35)] with N_s = 6 for increasing $\mathcal{T}$ (log scale) for the M_Σ^t and $M_\Sigma^\mathcal{T}$ schemes proposed herein, as well as those of M_Σ^{TP} (ref. 36) and M_Σ^{VES} (ref. 37). All simulations employed N_W = 6 and the collective variable $s = 2\pi x/l_x$. (c) As in (b), but using a finer grid of N_s = 48 bins of the CV. Each curve is an average over 32 independent MD/VES simulations, whose variations (data spread) are shown in Fig. S3 (ESI†). The horizontal red dotted lines in (b and c) mark the threshold of "sufficient" convergence, while the region around "near" convergence (dotted rectangle) is zoomed in the inset graphs (using a linear $\mathcal{T}$ scale). (d) Bias-correction function $c(t)$ associated with each reweighting protocol evaluated in (b) and shown for one representative simulation (see Section 5.4).

Fig. 6b plots the average D_{KL} response obtained from 32 independent simulations for increasing $\mathcal{T}$. We define $D_{KL} \leq 0.12$ as "sufficient" convergence, which is indicated by the dotted red line in Fig. 6b. As expected, D_{KL} evolves from its initial value ln{6}—*i.e.*, with all walkers confined to $\mathcal{D}_2$—to equally populated energy minima (D_{KL} = 0), as in Fig. 6a for $\mathcal{T}$ = 1.0 ns. The D_{KL} evolution among the various reweighting protocols vary significantly for increasing $\mathcal{T}$, with the value required to reach convergence ($\mathcal{T}_{conv}$) increasing according to $M_\Sigma^t < M_\Sigma^\mathcal{T} < M_\Sigma^{TP} < M_\Sigma^{VES}$, and translating into 150 ps, 170 ps, 240 ps, and 700 ps, respectively (Table 1). This corresponds to ≈4.6 times faster convergence of the "best" (M_Σ^t) scheme relative to the "worst" (M_Σ^{VES}). The relative convergence order remains essentially strict throughout all regions from "far" to "near", and "sufficient" convergence, except for M_Σ^{VES} (*vide infra*). Besides an overall slightly decelerated convergence of all methods, all findings concerning their relative merits also hold for the finer discretization with N_s = 48 shown in Fig. 6c. Morever, for the more stringent ("worst-case") convergence criterion that *all* 32 simulations from each method must reach convergence, Table 1 confirms a lower $\mathcal{T}_{conv}$ period required for M_Σ^t than any other reweighting scheme, thereby fully corroborating the inferences made from the alanine dipeptide evaluations.

Hence, the results of Fig. 6b,c and Table 1 suggest that the M_Σ^t protocol introduced herein outperforms its $M_\Sigma^\mathcal{T}$ counterpart, as well as both the Tiwary–Parrinello[36] and VES/BE[17,37] options. Notably, the performance of M_Σ^{VES} is remarkably poor for the present simple model system with a small walker ensemble, except for the $\mathcal{T} \leq 30$ ps domain far from any acceptable convergence threshold: in this $\mathcal{T}$-regime, the claim[37] of a more accurate reweighting than M_Σ^{TP} is indeed born out (yet, see Section 5.1.3). Fig. S3 (ESI†) presents the spread of $\{D_{KL}\}$ values observed among the N_{sim} = 32 simulations of each reweighting method of Fig. 6. The results are commensurate with those discussed for the alanine dipeptide (Fig. 5, and Fig. S1 and S2[ESI†]): the M_Σ^t, $M_\Sigma^\mathcal{T}$, and M_Σ^{TP} protocols reveal overall similar spreads, whereas that of VES/BE is typically wider.

Given that all our evaluations included the entire simulated trajectories in the reweighting, which may deteriorate the convergence of the methods based on CV integration (Sections 2.3.1 and 3.1), we also examined their "optimal" performance by locating t_{min} for each of M_Σ^{TP} and M_Σ^{VES}, whereupon the D_{KL} curves were re-evaluated, only retaining the simulated data beyond t_{min} for each N_s = {6, 48} scenario. Fig. S4 (ESI†) presents the results. Whereas essentially no improvement resulted for the M_Σ^{TP} method, a substantially enhanced performance is observed for M_Σ^{VES}, with the M_Σ^{TP} and M_Σ^{VES} methods now revealing the same convergence at $\mathcal{T}_{conv}$ = 230 ps for N_s = 6, and $\mathcal{T}_{conv}$ = 270 ps for N_s = 48. Although a significant time-span t < 100 ps of the simulated data was discarded, however, the M_Σ^{TP} and M_Σ^{VES} reweighting schemes remain inferior to M_Σ^t (Fig. S4 (ESI†) and Table 1). As expected, the data truncation gave no convergence improvements for any of the t-integration methods M_Σ^t and $M_\Sigma^\mathcal{T}$ (not shown). These results underscore the benefits of reweighting by time integration: no further efforts of locating the optimal t_{min}

 This journal is © the Owner Societies 2023

Open Access Article. Published on 03 July 2023. Downloaded on 1/21/2026 10:11:48 PM. This article is licensed under a Creative Commons Attribution 3.0 Unported Licence.

value are required, thereby also eliminating any potential systematic errors introduced by the data truncation[38] (Section 3.1). Yet, once undertaken for the CV-integration-based schemes, no dramatic differences are expected in the reweighting accuracy between *s*/*t*-integration-based methods.

5.3 Summary and further considerations

No single reweighting procedure is ever likely to outperform all others for MD simulations of any conceivable system and evaluation criterion. Yet the findings of Fig. 3–6 and Fig. S1–S4 (ESI†) altogether consolidate the M_Σ^t protocol as the method of choice for both large and small walker ensembles, regardless of (sub)optimal or "bad" choices of the CV: *at the worst* for a given modeled system, M_Σ^t is expected to deliver a comparable (or slightly inferior) reweighting accuracy compared with the globally best reweighting scheme. Worth underscoring is that VES/MD implementations employing time-integration-based estimates of the bias-correction function typically offer better accuracy and precision of the reweighted observable than the hitherto utilized standard VES reweighting[17–22] with $c(t) = 0$.

A (markedly) longer computational time for performing the reweighting constitutes a minor practical disadvantage of the novel time-integration $\{M_\mathcal{W}^\Gamma\}$ reweighting protocols relative to those utilizing CV averaging.[17,36,37] This feature, inherited from the ITRE protocol (see Giberti *et al.*[38]), is particularly pronounced for the $M_w^\mathcal{T}/M_\Sigma^\mathcal{T}$ schemes which estimate $c(t)$ by integration over the entire MD-simulation time-span. Table S1 (ESI†) contrasts the scaling of the number of floating-point operations required for each reweighting procedure evaluated herein, along with concrete CPU clock-timings for the simulations of Fig. 3a. Notably, however, these deficiencies of ITRE-derived protocols are in practice immaterial because the MD simulation (even for one walker) is orders-of-magnitude more time consuming than the subsequent reweighting stage, thereby rendering the time spent for the latter a largely irrelevant priority for selecting a reweighting protocol.

5.4 Analytical $c(t)$ expressions in the high-temperature limit

To gain further insight into the nature of the bias-correction functions, we consider a limiting high-temperature scenario of $\beta F(s) \ll 1$ and $\beta V(s, t) \ll 1$ with $\beta = (k_\mathrm{B}T)^{-1}$. Then, approximate analytical expressions may be obtained for the bias-correction function associated with each herein introduced $M_\mathcal{W}^\Gamma$ reweighting method, as well as that of Tiwary and Parrinello.[36]

For simulations with independent walkers, a Taylor expansion of the exponential functions of eqn (21) to first order yields

$$c_w^\Gamma(t) \approx \frac{\int_0^\Gamma \mathrm{d}\tau V(s_w(\tau), t)}{\int_0^\Gamma \mathrm{d}\tau\left[1 + \beta V(s_w(\tau), \tau) - \beta c_w^\Gamma(\tau)\right]} \approx \Gamma^{-1}\int_0^\Gamma \mathrm{d}\tau V(s_w(\tau), t), \quad \Gamma = \{t, \mathcal{T}\}, \tag{36}$$

which applies to one independent walker. Hence, $c_\mathrm{w}^\Gamma(t)$ is obtained as the time-average of the bias-potential taken up to either $\Gamma = t$ or $\Gamma = \mathcal{T}$. The same procedure applied to cooperative walkers [eqn (22)] yields a readily calculated average over the set of N_W correction functions $\{c_\mathrm{w}^\Gamma(t)\}$:

$$c_\Sigma^\Gamma(t) = N_\mathrm{W}^{-1}\sum_{w=1}^{N_\mathrm{W}} c_w^\Gamma(t). \tag{37}$$

We next consider the Tiwary–Parrinello reweighting protocol,[36] for which application of the high-temperature approximation to eqn (15) gives the following result:

$$\begin{aligned} c_\Sigma^\mathrm{TP}(t) \approx & \\ & -\beta^{-1}\left[\ln\left\{\int \mathrm{d}s\big(1 - \beta[F(s) + V(s,t)] + \beta^2[F(s) + V(s,t)]^2/2\big)\right\}\right. \\ & \left. -\ln\left\{\int \mathrm{d}s\big(1 - \beta F(s) + \beta^2 F(s)^2/2\big)\right\}\right] \\ & \approx \left\{\int \mathrm{d}s\, V(s,t)/\int \mathrm{d}s\right\} - \left\{\beta\int \mathrm{d}s V(s,t)[F(s) + V(s,t)/2]/\int \mathrm{d}s\right\}. \end{aligned} \tag{38}$$

When using well-tempered VES[17–19] with the bias potential of eqn (14), the integral $\int \mathrm{d}s V(s,t)/\int \mathrm{d}s$ in eqn (38) evaluates to $\alpha_0 = 0$, whereupon the bias-correction function may be expressed

$$c_\Sigma^\mathrm{TP}(t) \approx \frac{\beta(\gamma+1)}{4(\gamma-1)}\sum_{k=1}^{2N_\mathrm{F}}[\alpha_k(t)]^2 \tag{39}$$

in the high-temperature limit. Likewise, the BE reweighting[37] and its VES equivalent[17] implies that $c_\Sigma^\mathrm{VES}(t) = 0$ throughout (Section 2).

Albeit approximate, eqn (36)–(39) offer reasonably tractable analytical expressions of $c(t)$, as estimated by integration over either time[38] or over CVs.[36,37] For instance, Bonomi *et al.*[12] derived an equality between the time-derivatives of $c(t)$ and $\langle V(s, t)\rangle_s$, which follows trivially by applying either of eqn (36) or (39). We next consider the converged results of Fig. 6d, all of which provided $c_\Sigma^t(t) \approx c_\Sigma^\mathcal{T}(t) \approx c_\Sigma^\mathrm{TP}(t) \approx 1.92\,\mathrm{kJ\,mol^{-1}}$. (Because the function $c_\Sigma^\mathcal{T}(t)$ depends on the precise simulation period [eqn (22)], we employed $\mathcal{T} = 10.0\,\mathrm{ns}$ for the results plotted in Fig. 6d). Here, eqn (14), (31), and (39) with $\alpha_{11}(t) = -4.00\,\mathrm{kJ\,mol^{-1}}$ predict that $c_\Sigma^\mathrm{TP}(t) \approx [\alpha_{11}(t)]^2\beta(\gamma+1)/[4(\gamma-1)] = 2.32\,\mathrm{kJ\,mol^{-1}}$. Likewise, eqn (36) and (37) yield $c_\Sigma^t(t) \approx c_\Sigma^\mathcal{T}(t) \approx 2.32\,\mathrm{kJ\,mol^{-1}}$. Hence, in a minimum of computational efforts, the value of $c(t)$ for $t \to \infty$ is predicted with a relative error of 14% as compared with the accurate reference value of Fig. 6d.

6. Conclusions

We have generalized the recently proposed metadynamics ITRE reweighting protocol[38] to multiple-walker ensembles implemented within VES, moreover introducing and examining the usage of "independent" and "cooperative" walkers. For well-tempered VES simulations of two model cases, *viz.* the molecular conformations of *N*-acetyl-L-alanine methylamide, and a water molecule in the liquid phase subjected to a periodic free-energy function, we examined the relative merits of current state-of-the-art reweighting

Open Access Article. Published on 03 July 2023. Downloaded on 1/21/2026 10:11:48 PM. This article is licensed under a Creative Commons Attribution 3.0 Unported Licence.

methods introduced in the VES or metadynamics contexts[17,36,37] against four new options: the latter resulted by combining either independent or cooperative walkers with the bias-correction function $c(t)$ estimated by time integration up to either t or across the entire simulation period $\mathcal{T}$; see eqn (21) and (22).

The use of multiple-walker ES/MD simulations accelerates the convergence of the reweighted observables. For all but very small walker ensembles, the M_Σ^t and $M_\Sigma^\mathcal{T}$ methods that utilize cooperative walkers are superior to those with independent walkers (M_w^t and $M_w^\mathcal{T}$), with the performance-differences growing for increasing N_W. The precise upper time-integration limit of t (M_Σ^t) or $\mathcal{T}$ ($M_\Sigma^\mathcal{T}$) is not critical for $c(t)$ estimates for MD simulations with (moderately) large *cooperative* walker ensembles. For small walker ensembles ($N_\mathrm{W} < 8$), on the other hand, the advantages of cooperative walkers are minor compared to independent ones. Here, the choice of time-integration limit becomes much more critical—strongly favoring the M_Σ^t/M_w^t protocols relative to their $M_\Sigma^\mathcal{T}/M_w^\mathcal{T}$ counterparts—while the precise selection of "good" or "bad" collective variable(s) crucially underpins the convergence of all reweighting protocols.

Although no single reweighting protocol is expected to significantly outperform all others for any conceivable simulation scenario, out of the herein contrasted reweighting methods, the M_Σ^t scheme with cooperative walkers and the bias-correction function determined by time-integration up to t appears to be the overall most dependable option: it offers a superior accuracy for small walker ensembles than its primary and otherwise equivalent competitor ($M_\Sigma^\mathcal{T}$), along with much more rapid reweighting calculations. Notably, both multiple-walker M_Σ^t and $M_\Sigma^\mathcal{T}$ protocols are readily implemented in other ES methods, such as metadynamics. Moreover, we demonstrated that reweighting of VES-derived observables by the M_Σ^t procedure may be accelerated further by exploiting an analytical solution of its bias-correction function, as well as that qualitative insight into $c(t)$ may be gained by approximative analytical expressions in the "high-temperature" regime for all six reweighting protocols that were considered. Computer code for implementing the new reweighting procedures are available at **https://www.su.se/profiles/baltzar-1.187342** or may be obtained from the authors on request.

The herein recommended M_Σ^t scheme provides a better—or at worst comparable—reweighting accuracy as that of the currently best collective-variable-integration methods of Tiwary–Parrinello[36] (M_Σ^TP) and the "balanced exponential" (BE) of Schäfer and Settanni.[37] We demonstrated that when the BE reweighting is implemented within the VES framework, it becomes identical to the original VES implementation[17–20] (M_Σ^VES) with a constant bias-correction function. However, VES/BE reweighting often converged slower than the M_Σ^t, $M_\Sigma^\mathcal{T}$, and M_Σ^TP options, while typically giving a larger spread of reweighted observable-values between independent simulations. Albeit that deficiency may be alleviated by following the standard procedure of omitting the initial part of the simulated trajectory in the reweighting to improve accuracy, time-integration-based reweighting schemes offer decisive advantages by not requiring any such additional efforts/precautions along with their accompanying possible introduction of systematic errors. We conclude that enhanced reweighting of the VES/MD-derived observables are expected by embracing time-dependent $c(t) \neq 0$ options, such as the M_Σ^TP reweighting[36] and its time-integration M_Σ^t, $M_\Sigma^\mathcal{T}$ counterparts introduced herein.

Author contributions

BS – conceptualization, investigation, formal analysis and software; ME – funding acquisition and supervision; ME and BS – writing, original draft and revisions.

Conflicts of interest

There are no conflicts of interest to declare.

Acknowledgements

This work was supported by the Swedish Foundation for Strategic Research (funder ID 501100001729; project RMA15–0110), and in part by the Swedish Research Council (project VR 2022-03652). The computations were enabled by resources provided by the National Academic Infrastructure for Supercomputing in Sweden (NAISS) and the Swedish National Infrastructure for Computing (SNIC) at NSC, partially funded by the Swedish Research Council through grant agreements no. 2022-06725 and no. 2018-05973. We thank two anonymous reviewers for helpful suggestions that improved the manuscript.

References

1 G. M. Torrie and J. P. Valleau, Monte Carlo free energy estimates using non-Boltzmann sampling: Application to the sub-critical Lennard-Jones fluid, *Chem. Phys. Lett.*, 1974, **28**, 578–581.
2 G. M. Torrie and J. P. Valleau, Nonphysical sampling distributions in Monte Carlo free-energy estimation: Umbrella sampling, *J. Comput. Phys.*, 1977, **23**, 187–199.
3 U. H. E. Hansmann, Parallel tempering algorithm for conformational studies of biological molecules, *Chem. Phys. Lett.*, 1997, **281**, 140–150.
4 Y. Sugita and Y. Okamoto, Replica-exchange molecular dynamics method for protein folding, *Chem. Phys. Lett.*, 1999, **314**, 141–151.
5 S. Park and K. Schulten, Calculating potentials of mean force from steered molecular dynamics simulations, *J. Chem. Phys.*, 2004, **120**, 5946.
6 K. M. Bal, Reweighted Jarzynski sampling: Acceleration of rare events and free energy calculation with a bias potential learned from nonequilibrium work, *J. Chem. Theory Comput.*, 2021, **17**, 6766–6774.
7 A. Laio and M. Parrinello, Escaping free-energy minima, *Proc. Natl. Acad. Sci. U. S. A.*, 2002, **99**, 12562–12566.

Open Access Article. Published on 03 July 2023. Downloaded on 1/21/2026 10:11:48 PM. This article is licensed under a Creative Commons Attribution 3.0 Unported Licence.

8 A. Laio, A. Rodriguez-Fortea, F. L. Gervasio, M. Ceccarelli and M. Parrinello, Assessing the accuracy of metadynamics, *J. Phys. Chem. B*, 2005, **109**, 6714–6721.
9 G. Bussi, F. L. Gervasio, A. Laio and M. Parrinello, Free-energy landscape for β hairpin folding from combined parallel tempering and metadynamics, *J. Am. Chem. Soc.*, 2006, **128**, 13435–13441.
10 A. Laio and F. L. Gervasio, Metadynamics: a method to simulate rare events and reconstruct the free energy in biophysics, chemistry and material science, *Rep. Prog. Phys.*, 2008, **71**, 126601.
11 A. Barducci, G. Bussi and M. Parrinello, Well-tempered metadynamics: A smoothly converging and tunable free-energy method, *Phys. Rev. Lett.*, 2008, **100**, 020603.
12 M. Bonomi, A. Barducci and M. Parrinello, Reconstructing the equilibrium Boltzmann distribution from well-tempered metadynamics, *J. Comp. Chem.*, 2009, **30**, 1615–1621.
13 M. Bonomi and M. Parrinello, Enhanced sampling in the well-tempered ensemble, *Phys. Rev. Lett.*, 2010, **104**, 190601.
14 A. Barducci, M. Bonomi and M. Parrinello, Metadynamics, *Wiley Interdiscip. Rev.: Comput. Mol. Sci.*, 2011, **1**, 826–843.
15 J. F. Dama, M. Parrinello and G. A. Voth, Well-tempered metadynamics converges asymptotically, *Phys. Rev. Lett.*, 2014, **112**, 240602.
16 G. Bussi and A. Laio, Using metadynamics to explore complex free-energy landscapes, *Nat. Rev. Phys.*, 2020, **2**, 200–212.
17 O. Valsson and M. Parrinello, Variational approach to enhanced sampling and free energy calculations, *Phys. Rev. Lett.*, 2014, **113**, 090601.
18 O. Valsson and M. Parrinello, Well-tempered variational approach to enhanced sampling, *J. Chem. Theory Comput.*, 2015, **11**, 1996–2002.
19 O. Valsson, P. Tiwary and M. Parrinello, Enhancing important fluctuations: Rare events and metadynamics from a conceptual viewpoint, *Annu. Rev. Phys. Chem.*, 2016, **67**, 159–184.
20 O. Valsson and M. Parrinello, Variationally enhanced sampling, in *Handbook of Materials Modeling*, ed. W. Andreoni and S. Yip, Springer, Cham, 2020, pp. 621–634.
21 P. M. Piaggi, O. Valsson and M. Parrinello, A variational approach to nucleation simulation, *Faraday Discuss.*, 2016, **195**, 557–568.
22 P. Shaffer, O. Valsson and M. Parrinello, Enhanced, targeted sampling of high-dimensional free-energy landscapes using variationally enhanced sampling, with an application to chignolin, *Proc. Natl. Acad. Sci. U. S. A.*, 2016, **113**, 1150–1155.
23 Y. I. Yang and M. Parrinello, Refining collective coordinates and improving free energy representation in variational enhanced sampling, *J. Chem. Theory Comput.*, 2018, **14**, 2889–2894.
24 L. Mones, N. Bernstein and G. Csányi, Exploration, sampling, and reconstruction of free energy surfaces with Gaussian process regression, *J. Chem. Theory Comput.*, 2016, **12**, 5100–5110.
25 L. Bonati, V. Rizzi and M. Parrinello, Data-driven collective variables for enhanced sampling, *J. Phys. Chem. Lett.*, 2020, **11**, 2998–3004.
26 J. Rydzewski and O. Valsson, Multiscale reweighted stochastic embedding: Deep learning of collective variables for enhanced sampling, *J. Phys. Chem. A*, 2021, **125**, 6286–6302.
27 M. Invernizzi, P. M. Piaggi and M. Parrinello, Unified approach to enhanced sampling, *Phys. Rev. X*, 2020, **10**, 041034.
28 Q. Liao, Chapter four-enhanced sampling and free energy calculations for protein simulations, *Prog. Mol. Biol. Trans. Sci.*, 2020, **170**, 177–213.
29 R. Demuynck, S. M. J. Rogge, L. Vanduyfhuys, J. Wieme, M. Waroquier and V. Van Speybroeck, Efficient construction of free energy profiles of breathing metal-organic frameworks using advanced molecular dynamics simulations, *J. Chem. Theory C*, 2017, **13**, 5861–5873.
30 B. Pampel and O. Valsson, Improving the efficiency of variationally enhanced sampling with wavelet-based bias potentials, *J. Chem. Theory Comput.*, 2022, **18**, 4127–4141.
31 K. M. Bal and E. C. Neyts, Merging metadynamics into hyperdynamics: Accelerated molecular simulations reaching time scales from microseconds to seconds, *J. Chem. Theory Comput.*, 2015, **11**, 4545–4554.
32 P. Kříž, Z. Šućur and V. Spiwok, Free-energy surface prediction by flying Gaussian method: Multisystem representation, *J. Phys. Chem. B*, 2017, **121**, 10479–10483.
33 S. Kumar, D. Bouzida, R. H. Swendsen, P. A. Kollman and J. M. Rosenberg, The weighted histogram analysis method for free-energy calculations on biomolecules. I. The method, *J. Comput. Chem.*, 1992, **13**, 1011–1021.
34 B. Roux, The calculation of the potential of mean force using computer simulations, *Comput. Phys. Comm.*, 1995, **91**, 275–282.
35 L. Donati and B. G. Keller, Girsanov reweighting for metadynamics simulations, *J. Chem. Phys.*, 2018, **149**, 072335.
36 P. Tiwary and M. Parrinello, A time-independent free energy estimator for metadynamics, *J. Phys. Chem. B*, 2015, **119**, 736–742.
37 T. M. Schäfer and G. Settanni, Data reweighting in metadynamics simulations, *J. Chem. Theory Comput.*, 2020, **16**, 2042–2052.
38 F. Giberti, B. Cheng, G. A. Tribello and M. Ceriotti, Iterative unbiasing of quasi-equilibrium sampling, *J. Chem. Theory Comput.*, 2020, **16**, 100–107.
39 F. Pietrucci, Strategies for the exploration of free energy landscapes: Unity in diversity and challenges ahead, *Rev. Phys.*, 2017, **2**, 32–45.
40 S. K. Veesam, S. Ravipati and S. N. Punnathanam, Recent advances in thermodynamics and nucleation of gas hydrates using molecular modeling, *Curr. Opin. Chem. Eng.*, 2019, **23**, 14–20.
41 S. Fukuhara, K. M. Bal, E. C. Neyts and Y. Shibuta, Accelerated molecular dynamics simulation of large systems with parallel collective variable-driven hyperdynamics, *Comp. Mat. Sci.*, 2020, **177**, 109581.
42 J. J. Varghese and S. H. Mushrif, Origins of complex solvent effects on chemical reactivity and computational tools to investigate them: a review, *React. Chem. Eng.*, 2019, **4**, 165.
43 S. Xu and E. A. Carter, Theoretical insights into heterogeneous (photo)electrochemical CO_2 reduction, *Chem. Rev.*, 2019, **119**, 6631–6669.

Open Access Article. Published on 03 July 2023. Downloaded on 1/21/2026 10:11:48 PM.
This article is licensed under a Creative Commons Attribution 3.0 Unported Licence.

44 P. Liu and D. Mei, Identifying free energy landscapes of proton-transfer processes between Brønsted acid sites and water clusters inside the zeolite pores, *J. Phys. Chem. C*, 2020, **124**, 22568–22576.
45 J. Coines, L. Raich and C. Rovira, Modeling catalytic reaction mechanisms in glycoside hydrolases, *Curr. Opin. Chem. Biol.*, 2019, **53**, 183–191.
46 P. Ibrahim and T. Clark, Metadynamics simulations of ligand binding to GPCRs, *Curr. Opin. Struct. Biol.*, 2019, **55**, 129–137.
47 A. V. Dongre, S. Das, A. Bellur, S. Kumar, A. Chandrashekarmath, T. Karmakar, P. Balaram, S. Balasubramanian and H. Balaram, Structural basis for the hyperthermostability of an archaeal enzyme induced by succinimide formation, *Biophys. J.*, 2021, **120**, 3732–3746.
48 Z. Xu, Y. Yang, Z. Wang, D. Mkhonto, C. Shang, Z.-P. Liu, Q. Cui and N. Sahai, Small molecule-mediated control of hydroxyapatite growth: Free energy calculations benchmarked to density functional theory, *J. Comput. Chem.*, 2014, **35**, 70–81.
49 Q. Wang, M. Wang, K. Wang, Y. Liu, H. Zhang, X. Lu and X. Zhang, Computer simulation of biomolecule-biomaterial interactions at surfaces and interfaces, *Biomed. Mater.*, 2015, **10**, 032001.
50 H. Heinz and H. Ramezani-Dakhel, Simulations of inorganic-bioorganic interfaces to discover new materials: insights, comparisons to experiment, challenges, and opportunities, *Chem. Soc. Rev.*, 2016, **45**, 412–448.
51 J. McCarty, O. Valsson, P. Tiwary and M. Parrinello, Variationally optimized free-energy flooding for rate calculation, *Phys. Rev. Lett.*, 2015, **115**, 070601.
52 P. Shaffer, O. Valsson and M. Parrinello, Hierarchical protein free energy landscapes from variationally enhanced sampling, *J. Chem. Theory Comput.*, 2016, **12**, 5751–5757.
53 P. Raiteri, A. Laio, F. L. Gervasio, C. Micheletti and M. Parrinello, Efficient reconstruction of complex free energy landscapes by multiple walkers metadynamics, *J. Phys. Chem. B*, 2006, **110**, 3533–3539.
54 F. Giberti, G. A. Tribello and M. Ceriotti, Global free-energy landscapes as a smoothly joined collection of local maps, *J. Chem. Theory Comput.*, 2021, **17**, 3292–3308.
55 M. P. Allen and D. J. Tildesley, *Computer Simulation of Liquids*, Clarendon Press, Oxford, 1987.
56 L. Molgedey and H. G. Schuster, Separation of a mixture of independent signals using time delayed correlations, *Phys. Rev. Lett.*, 1994, **72**, 3634–3637.
57 B. Stevensson and M. Edén, Metadynamics simulations of the pH-dependent adsorption of phosphoserine and citrate on disordered apatite surfaces: What interactions govern the molecular binding?, *J. Phys. Chem. B*, 2021, **125**, 11987–12003.
58 R. Mathew, B. Stevensson, M. Pujari-Palmer, C. S. Wood, P. R. A. Chivers, C. D. Spicer, H. Autefage, M. M. Stevens, H. Engqvist and M. Edén, Nuclear magnetic resonance and metadynamics simulations reveal the atomistic binding of L-serine and *O*-phospho-L-serine at disordered calcium phosphate surfaces of biocements, *Chem. Mater.*, 2022, **34**, 8815–8830.
59 M. J. Abraham, T. Murtola, R. Schulz, S. Páll, J. C. Smith, B. Hess and E. Lindahl, GROMACS: High performance molecular simulations through multi-level parallelism from laptops to supercomputers, *SoftwareX*, 2015, **1–2**, 19–25.
60 U. Essmann, L. Perera, M. L. Berkowitz, T. Darden, H. Lee and L. G. Pedersen, A smooth particle mesh Ewald method, *J. Chem. Phys.*, 1995, **103**, 8577–8593.
61 G. Bussi, D. Donadio and M. Parrinello, Canonical sampling through velocity rescaling, *J. Chem. Phys.*, 2007, **126**, 014101.
62 G. A. Tribello, M. Bonomi, D. Branduardi, C. Camilloni and G. Bussi, PLUMED 2: New feathers for an old bird, *Comput. Phys. Comm.*, 2014, **185**, 604–613.
63 F. Bach and E. Moulines, Non-strongly-convex smooth stochastic approximation with convergence rate $O(1/n)$, in *Advances in neural information processing systems*, ed. C. J. C. Burges, L. Bottou, M. Welling, Z. Ghahramani, and K. Q. Weinberger, Curran Associates, Inc., Red Hook, NY, 2013, vol. 26, pp. 773–781.
64 P. Bjelkmar, P. Larsson, M. A. Cuendet, B. Hess and E. Lindahl, Implementation of the CHARMM force field in GROMACS: Analysis of protein stability effects from correction maps, virtual interaction sites, and water models, *J. Chem. Theory Comput.*, 2010, **6**, 459–466.
65 B. Efron and C. Stein, The jackknife estimate of variance, *Ann. Statist.*, 1981, **9**, 586–596.
66 W. L. Jorgensen, J. Chandrasekhar, J. D. Madura, R. W. Impey and M. L. Klein, Comparison of simple potential functions for simulating liquid water, *J. Chem. Phys.*, 1983, **79**, 926–935.
67 S. Kullback and R. A. Leibler, On information and sufficiency, *Annals Math. Stat.*, 1951, **22**, 79–86.